

Seismic Measurements on the Ocean Floor

1. Bermuda Area¹

GARY V. LATHAM AND GEORGE H. SUTTON²

*Lamont Geological Observatory, Columbia University
Palisades, New York*

A seismograph system was placed on the ocean floor 65 km south of Bermuda in May 1964, at a depth of 4.3 km. Instrumentation consisted of three long-period seismometers (natural period = 15 sec) and one short-period vertical-component seismometer (natural period = 1 sec). Data were telemetered acoustically to a shipborne receiver for 8½ days. This experiment represents the first successful attempt to operate long-period seismographs on the ocean floor. Predominant periods, time variations in average level, and associated energy flux of observed microseisms are approximately the same at Bermuda and on the ocean floor. It is concluded that (1) the energy of the microseisms is coupled into the layered medium by water-wave interaction, (2) the observed microseisms were generated near Bermuda and not directly beneath storms at sea, and (3) these microseisms propagate primarily as Rayleigh waves of the fundamental mode. Phases from nine earthquakes were identified on the records from the ocean-bottom instruments. The general character of the observed phases does not differ substantially from those recorded at the Bermuda standard station except for the presence of greater high-frequency amplitudes on the ocean bottom from a series of Dominican Republic shocks. The signal-to-noise ratio is larger at Bermuda for periods longer than about 1 sec, but is larger at the ocean-bottom site for shorter periods. Energy associated with a short-period Rayleigh wave propagating through the ocean bottom in the fundamental mode is concentrated near the water-sediment interface. In the island structure, the energy is distributed more uniformly with depth. This difference explains the relatively large microseismic amplitudes measured on the ocean floor. On the basis of the model used to represent the structure at the ocean-bottom site, for a given energy flux, removal of the unconsolidated sediment layer reduces the theoretical particle-motion amplitude of the water-solid interface by factors of 8 and 94 for the vertical and horizontal components, respectively. Such a reduction in background level would make the ocean-bottom site an order of magnitude quieter than the station on Bermuda. This result indicates the possible advantages of locating instruments at sediment-free sites on the ocean bottom.

INTRODUCTION

Results obtained from a four-component seismograph system which operated successfully on the ocean bottom 65 km south of Bermuda, at a depth of 4.3 km, are described. The experiment was conducted between May 25 and June 2, 1964, by Lamont Geological Observatory personnel. Uninterrupted seismic data were obtained for 8½ days.

The first successful attempts to operate a seismograph on the ocean bottom at great depths were made by Ewing and associates in 1937 and 1938 [Ewing and Vine, 1938]. These

early instruments were intended primarily for use in seismic refraction work. This work and the subsequent experiments conducted by Ewing and colleagues have been summarized by Ewing and Ewing [1961] and Prentiss and Ewing [1963]. Other groups have recently become active in this field [Schneider, 1964; Bradner, 1964; Monakhov, 1962]. These studies have produced many important results. It has been established that the ocean bottom is not, in general, a quiet recording site compared with land locations. Microseismic amplitudes on the ocean bottom are as much as an order of magnitude larger than those measured at nearby land sites. It has been shown, however, that the high-frequency energy content of earthquake seismograms recorded on the ocean bottom is often much

¹ Lamont Geological Observatory Contribution 898.

² Also Department of Geology, Columbia University.

larger than in seismograms recorded on land. Thus the ocean bottom can be a superior recording site at frequencies greater than 1 cps. There is also limited evidence that microseisms consist of normal mode waves.

Although they have yielded valuable data, each of these studies had two basic limitations: (1) the seismometers employed all had short natural periods (1 sec or less) and (2) the duration of one continuous recording was relatively short (from several minutes to 72 hours). As a result, the signal spectrum at periods longer than about 4 to 5 sec has not been well determined. Also, short-term recording does not lend itself to an understanding of the variations in microseismic activity with time.

To overcome the limitations of the earlier programs, the development of a long-period seismograph system for use on the ocean bottom was undertaken at Lamont Geological Observatory in 1964. The instrument system was installed in late April 1965, 170 km off the coast of northern California. Data are transmitted by cable to the recording station at Point Arena, California. A detailed description of the instrumentation and first results from the data are given by *Sutton et al.* [1965]. The ocean-bottom installation near Bermuda was intended to serve as a system test in preparation for the permanent installation off the California coast.

1. INSTRUMENTATION AND FIELD OPERATION

The primary elements of the instrument system are (1) a three-component set of pendulums with 15-sec natural periods; (2) one short-period vertical-component seismometer (SPZ) with natural period of 1 sec; (3) an acoustic telemetry system including a transmitter-receiver with the instrument system below and on the listening ship above; (4) command electronics which permits execution of such functions as cage release and recage, turning transmitter power on and off, change of gain, calibration, and seismometer leveling by command from the listening ship; (5) a mercury battery power pack attached to the ocean-bottom unit; and (6) demultiplexing electronics and a recording system located on the listening ship. These elements are described in greater detail by *Sutton et al.* [1965].

The three long-period pendulums are mounted

in a motor-driven leveling gimbal. A separate motor centers the long-period vertical-component seismometer (LPZ) by raising or lowering the upper suspension point of the main spring. The seismometers have capacitance-type transducers and feedback control for greater long-term stability, as described by *Sutton and Latham* [1964].

The SPZ is a modified Hall-Sears model HS-10 with a natural period of 1 sec. This unit has a self-generating coil-magnet transducer. The seismometer is mounted on the underside of the gimbal so that it is leveled when the long-period pendulums are leveled.

Data were transmitted to the surface by means of a hydroacoustic link operating on telemetry channel 12 (10.5 kc/s) with an average acoustic power of 2.5 watts. The telemetry system is described in detail by *Thanos and Hubbard* [1966].

The power supply consisted of low-temperature mercury cells which were sufficient to power the system for a minimum of 15 days of continuous operation. The batteries were packed into a spherical aluminum pressure vessel 55 cm in diameter and 2.5 cm thick. The seismometers and associated electronics were fitted into another pressure vessel of the same dimensions. The two spheres were mounted in a steel tripod, each leg being terminated with a large aluminum disk to prevent the unit from sinking into soft sediments.

Data were received by the listening ship and recorded on magnetic tape and on a 4-channel chart recorder which served as a continuous monitor. Magnification curves for all four instruments are shown in Figure 1 along with those for standard station instruments located on Bermuda (BDA). The ocean-bottom seismograph (OBS) curves apply to the signal as recorded on the 4-channel chart recorder (seismometers set at medium gain, chart recorder sensitivity = 1 v/cm).

The inertial mass of one of the horizontal-component seismometers remained clamped during the experiment. The output from this channel was a steady tone at 10.5 kc/s. However, the frequency detected by the shipborne receiver varied continuously as a function of the relative velocity between the ship and the transmitter (Doppler effect). If the ship motion followed water particle motion, the Doppler

shift in the tone from the inoperative seismometer directly was thus related to the amplitude of water waves. Water-wave records obtained from Doppler-shift data are discussed in section 4.

The arrival time of a seismic signal at the shipborne receiver is delayed by the travel time in the water layer; hence arrival times at the ocean-bottom site are known only to the accuracy that the distance between transmitter and ship is known. It is estimated that the listening ship was never more than 2.4 km from the point directly over the transmitter and usually no more than 1.2 km. The appropriate time correction required to compensate for water-wave travel time is thus -3.0 ± 0.2 sec.

2. RECORDING SITE

As shown in Figure 2, the OBS was located near the base of the southern flank of the Bermuda pedestal ($31^{\circ}40.8'N$, $64^{\circ}45.8'W$) at a depth of 2340 fathoms (4.3 km). The following regional description is excerpted primarily from *Heezen et al.* [1959]. The islands of Bermuda lie along the southwest rim of a flat-topped volcanic pedestal whose surface lies generally less than 40 meters below sea level. The sides of the pedestal fall steeply to its base, which is at a depth of about 4.2 km. The size of the pedestal base is approximately 80 km by 130 km. The pedestal rises up from a much larger feature called the Bermuda rise, which is an oval arch extending about 500 by 1000 km, with the long axis oriented NE-SW. The average depth of water over this feature is approximately 4.6 km. The Bermuda rise, in turn, is bounded by abyssal plains and hills.

On the Bermuda rise—a typical oceanic crust—we are dealing with four principal layers overlying the mantle: (1) water, (2) unconsolidated sediments, (3) basement, consisting of consolidated sediments and volcanic material near Bermuda, and (4) oceanic crust.

The unconsolidated sediment layer in the region of the seismometer site was mapped by the reflection profiler technique during *Vema* cruise 18, in December 1961. This technique is described by *Ewing and Tirey* [1961], and the records were made available to us by J. Ewing. The sediment structure traced from these profiler records is shown in Figure 3. The track

along which the profile is located is shown in Figure 2 (track A-A'). The instrument is located on a thickness of about 0.3 km of sediments 20 to 25 km south of the point where the sediments pinch out against the southern flank of the Bermuda pedestal. The sediment layer thickens southward to about 0.45 km and then gradually becomes thinner.

Houtz and Ewing [1964] studied the sediments in the western North Atlantic by means of both refraction and reflection seismic techniques. Their results show that velocity gradients in the sediment layer are variable and are greatest near the water-sediment interface. On the basis of data from 60 profiles, they propose the following relation between sediment compressional wave velocity v and depth h :

$$v = v_0 \left[1 + \frac{kh(n+1)}{v_0 n} \right]^{1/(n+1)} \quad (1)$$

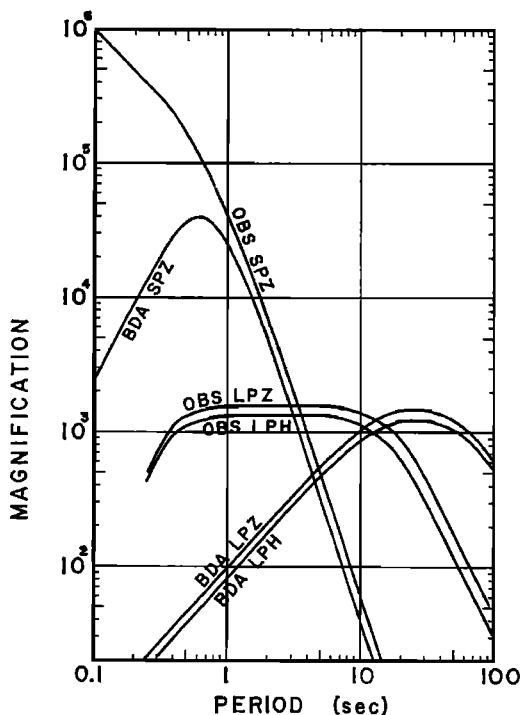


Fig. 1. Magnification curves for (1) the vertical and horizontal components of the long-period ocean-bottom seismograph (OBS LPZ, OBS LPH); (2) the short-period ocean-bottom seismograph (OBS SPZ); (3) the Bermuda standard station long-period vertical-, long-period horizontal-, and short-period vertical-component seismographs (BDA LPZ, BDA LPH, BDA SPZ).

where $n = 5$, $k = 8.75$, and $v_0 = 1.52$ km/sec. For these parameter values, (1) becomes

$$v = 1.52(1 + 6.91h)^{1/6} \text{ km/sec} \quad (h \text{ in km}) \quad (2)$$

Accepting this relation as valid for the region near Bermuda, we can compute velocity as a function of depth in the sediment. The associated densities and shear velocities can be derived from data given by *Nafe and Drake* [1963].

The parameters of the layered structure

taken to represent the OBS site are listed in Table 1 (model 4-B). Other models listed in Table 1 (except 7-B) represent small departures from the standard model. These auxiliary models will show the effects of small changes in structure on Rayleigh wave propagation (section 5).

For purposes of computation, the sedimentary column has been arbitrarily divided into four homogeneous layers. The top layer is 0.01 km thick and each of the three lower layers is 0.1 km thick. The low shear velocities shown

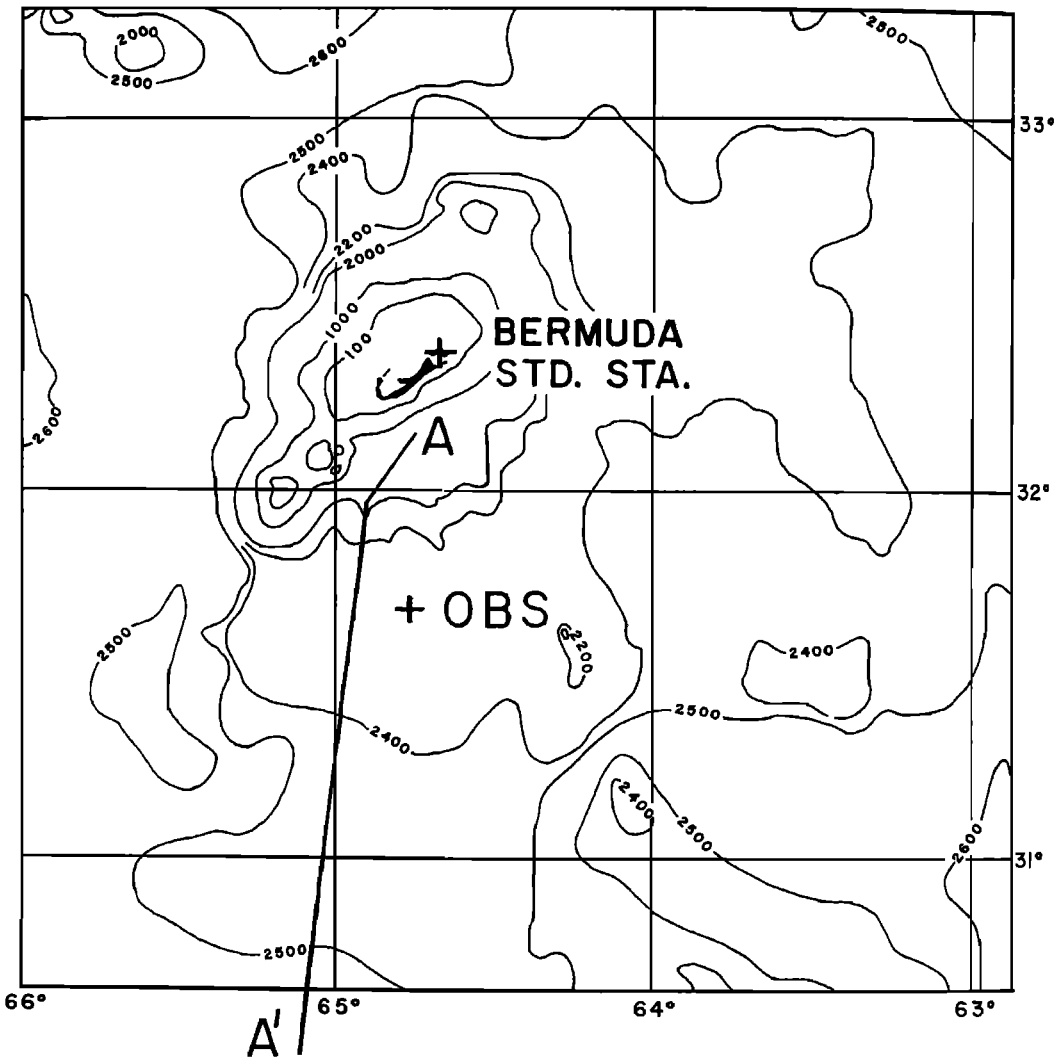


Fig. 2. Bathymetric map showing the Bermuda pedestal, the OBS site, and the location of the sediment profile (A-A') shown in Figure 3. Contour units are fathoms.

are consistent with values proposed by *Sykes and Oliver* [1964a, b] and *Oliver and Dorman* [1961] to explain short-period oceanic surface waves. The remainder of the model was derived from the structure sections for the western North Atlantic given by *Houtz and Ewing* [1963]. The mantle is assumed to be a half-space.

Model 7-B (Table 1), representing the island structure, was derived primarily from *Katz and Ewing* [1956]. The depth to the base of the volcanic pedestal is taken to be 21 km to satisfy the requirement that the average density from the surface to a depth of 32 km be equal to 2.87 g/cm^3 as required by regional gravity data (M. Talwani, personal communication, 1964) if perfect isostatic balance is assumed. The density at the top of the mantle is assumed to be 3.4 g/cm^3 . *Woollard* [1954] and *Phinney* [1964] found smaller depths to the Mohorovicic discontinuity in their work, but this simplified model is adequate for the present purposes because we will be concerned primarily with the upper 10 km. It is admittedly a simplification to assume that the sedimentary layers are of uniform thickness in this region. Any results which depend on this assumption must be qualified accordingly.

3. MICROSEISMS, GENERAL DESCRIPTION

A typical sample of microseisms as recorded by the OBS is shown in Figure 4. Several points are immediately apparent. The amplitudes are large relative to those of normal land record-

ings, and the horizontal amplitudes are noticeably larger than the vertical amplitudes. Maximum amplitudes were 30μ and 7μ peak to peak for the horizontal and vertical components, respectively. These compare with amplitudes of 3.5μ and 2.5μ for horizontal and vertical motion, respectively, recorded at the standard station on Bermuda. These amplitudes were recorded under relatively quiet sea conditions (rms wave height at the recording station $\approx 20 \text{ cm}$). The average ratio of horizontal-to-vertical particle-motion amplitude ranges between 3.0 and 4.0, whereas for Bermuda the value is approximately unity. The periods range between 3.5 and 4.0 sec with peak energy at about 3.7 to 3.8 sec.

The typical 'beat,' or group, seen on land station records is well developed on the ocean bottom. However, a well-defined beat on the record for the horizontal component is not necessarily associated with a similar feature on the record for the vertical component; i.e., the coherence between components is quite low. The coherence of microseisms recorded at Bermuda during this period was also low. A sample of the island microseisms is not shown because the record amplitudes are too small to be adequately reproduced.

The signal from the inoperative seismometer derives primarily from the Doppler-shift effect described earlier, plus a small amount of system noise.

Microseismic amplitudes and periods were measured every 6 hours for both the OBS rec-

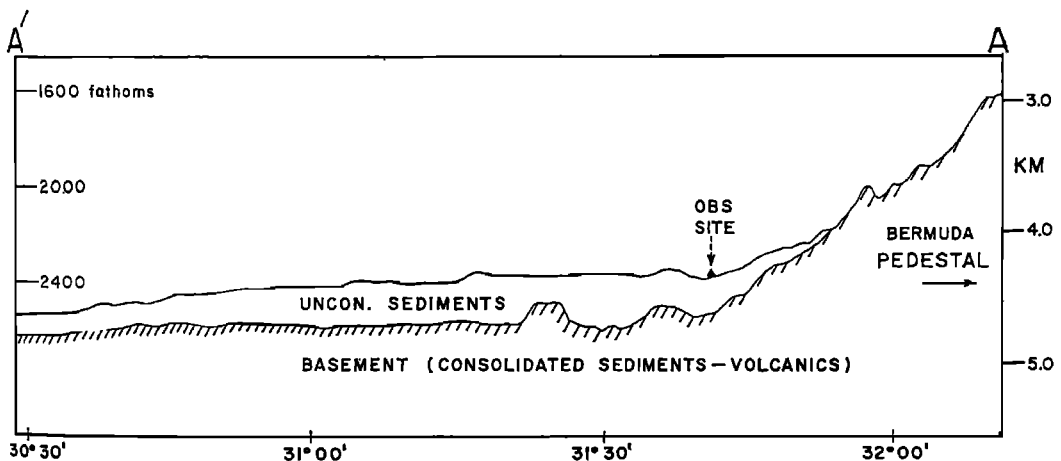


Fig. 3. Profile of sediment layer and basement topography in the vicinity of the OBS site.

TABLE 1. Layer Parameters for Oceanic and Island Crustal Models
(α , β , ρ are the compressional velocity, shear velocity, and density, respectively.)

Model	Layer Thickness, km	α , km/sec	β , km/sec	ρ , g/cm ³
3-B	4.40	1.52	0.00	1.03
	0.10	1.60	0.19	1.70
	0.10	1.71	0.37	1.79
	0.10	1.80	0.53	1.86
	1.30	4.73	2.74	2.50
	5.10	6.65	3.74	2.81
	∞	8.04	4.42	3.40
4-B	4.40	1.52	0.00	1.03
	0.01	1.52	0.15	1.65
	0.10	1.60	0.19	1.70
	0.10	1.71	0.37	1.79
	0.10	1.80	0.53	1.86
	1.30	4.73	2.74	2.50
	5.10	6.65	3.74	2.81
∞	8.04	4.60	3.40	
5-B	4.40	1.52	0.00	1.03
	0.10	1.60	0.19	1.70
	0.10	1.71	0.37	1.79
	0.10	1.80	0.53	1.86
	0.20	2.00	0.74	1.93
	1.30	4.73	2.74	2.50
	5.10	6.65	3.74	2.81
∞	8.04	4.42	3.40	
6-B	5.00	1.52	0.00	1.03
	0.10	1.60	0.19	1.70
	0.10	1.71	0.37	1.79
	0.10	1.80	0.53	1.86
	1.30	4.73	2.74	2.50
	5.10	6.65	3.74	2.81
	∞	8.04	4.42	3.40
7-B	0.08	2.70	1.56	2.15
	21.00	5.25	3.00	2.60
	∞	8.04	4.42	3.40
8-B	4.40	1.52	0.00	1.03
	0.01	1.52	0.15	1.65
	0.10	1.60	0.19	1.70
	0.10	1.71	0.37	1.79
	0.10	1.80	0.53	1.86
	2.30	4.73	2.74	2.50
	5.10	6.65	3.74	2.81
∞	8.04	4.60	3.40	

ords and the BDA records. In measuring amplitudes, an attempt was made to estimate the peak-to-peak level not exceeded more than 10% of the time. Amplitudes measured on the standard station records were quite small (maximum of 1.2 mm), so that the accuracy of the measurements is of the order of $\pm 20\%$. The results of this semiquantitative analysis

are shown in Figure 5. The much greater amplitudes at the ocean-bottom site are immediately obvious. The predominant period, however, is very nearly the same at the two sites. The temporal variations in average amplitude are also similar at the two sites. It is clear that a genetic relationship exists between microseisms measured on the ocean bottom and those measured on Bermuda. Data for the Bermuda LPH in Figure 5 were obtained from the E-W component.

Weather maps which cover the entire North Atlantic area were studied to determine whether the peaks in microseismic activity could be correlated with the passage of weather systems. The maps used are produced every 6 hours by the San Juan division of the United States Weather Bureau. Two small storm systems passed near Bermuda during the recording period, and their tracks are shown in Figure 6. Since these were the only storms that passed in the vicinity of Bermuda during the recording period, and since their times of closest approach to the island corresponded roughly to the times of peak activity, there seems little doubt that the two peaks in microseismic activity are associated with these weather systems.

The first weather system was a weak trough of low pressure which trended N-S, with a

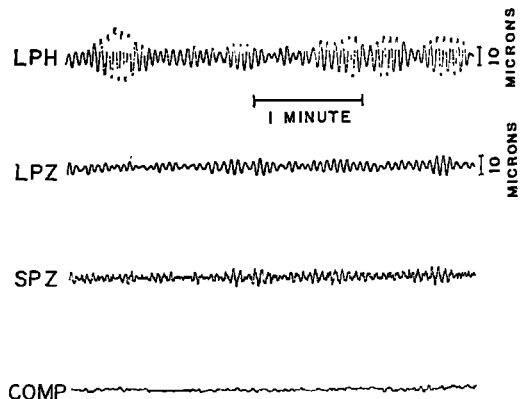


Fig. 4. A sample of microseism signal recorded by the ocean-bottom seismograph. LPH = long-period horizontal-component seismograph; LPZ = long-period vertical-component seismograph; SPZ = short-period vertical-component seismograph; and COMP = output from the inoperative horizontal component. Recorded May 29, 1964, at 1500 UT.

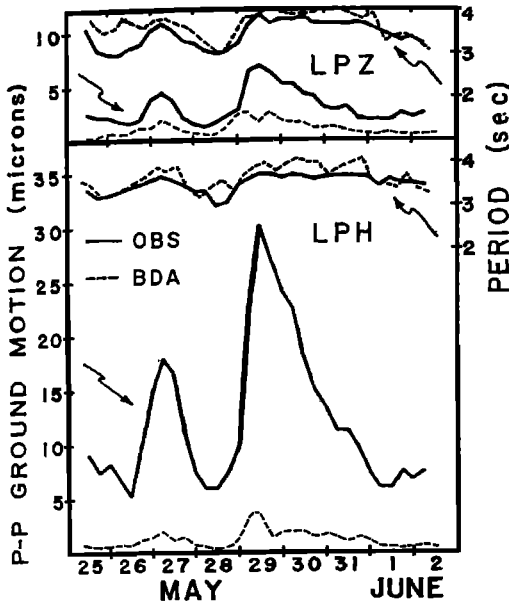


Fig. 5. Time dependence of the period and amplitude of microseisms at the ocean-bottom site and at the Bermuda standard station for the vertical-component seismograph and the horizontal-component seismograph.

poorly developed low-pressure center moving along the trough. The center of this low-pressure area is indicated along the track by short transverse lines. The trend of a line serves as a rough indication of the trend of the front at the indicated time. The weak trough and associated low are first seen in the weather maps of May 25, 1200 UT; the low centered 800 km south of Bermuda, and the trough trended NE-SW to the east of Bermuda. They are closest to Bermuda and the OBS site on the map for May 27, 0000 UT. At this time, the trough had extended northward to join a cold front. The maximum microseismic amplitudes on the ocean bottom were recorded at about 0300 UT, May 27. Subsequently, the trough and low moved off rapidly to the east and the microseisms diminished.

The second weather system consisted of a cold front extending southward in a long arc from a nearly stationary, intense low-pressure system centered near Newfoundland. A secondary low formed along the cold front and moved eastward from the coast of the United States toward the region north of Bermuda. The microseisms recorded on the OBS are

plotted at the corresponding time along the track. The peak amplitudes at the OBS were recorded at about 1200 UT on May 29, which was somewhat before the time of closest approach of the center of the secondary low to Bermuda. However, the assignment of a point to designate the storm position can be misleading, especially in dealing with a secondary low elongated along the frontal zone. The point which is taken to be the storm position is the location of minimum pressure at the seaward end of the elongated secondary low. This point is not well defined and, in any case, may not be the most important point with regard to the generation of microseisms.

4. POWER SPECTRUMS

We considered the microseism background to be a quasi-stationary random signal and computed the power density spectrum [Blackman and Tukey, 1958]. Five time intervals were chosen for analysis. The beginning time for each section is listed in Table 2. Samples are 30 min long for data from the long-period instruments. Samples 2 and 4 were chosen to coincide with the two peaks in microseismic activity. Samples 1, 3, and 5 occur before, between, and after the periods of peak activity. The spectrums described below each have ap-

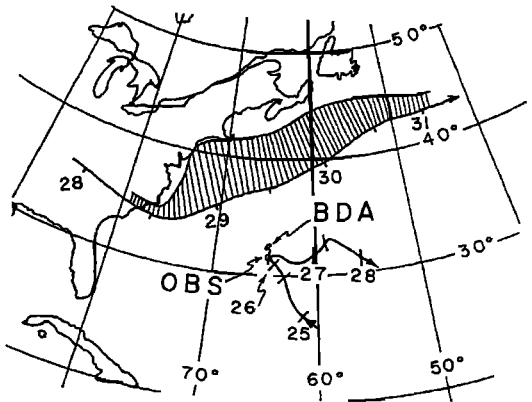


Fig. 6. Tracks of the two weather systems associated with peaks in microseism activity. Tick marks on the track indicate the center of the weather system at 0000 and 1200 hours (UT). The date is given at the 1200-hour mark. The width of the hatched area along the northern track at a given time is proportional to the amplitudes of microseisms recorded on the ocean bottom at the corresponding time.

TABLE 2. Periods, rms Amplitudes and Q Values for Microseisms and Water Waves at the Ocean Bottom Seismograph (OBS) Site and the Bermuda Standard Station (BDA)

Sample	Site	May 1964	Hour, UT	LPZ*			LPH†			Water Waves		
				Period, sec	rms, microns	Q	Period, sec	rms, microns	Q	Period, sec	rms, cm	Q
1	OBS	25	1400	3.4	0.63	3.5	3.4	1.90	5.3	7.1	11.9	3.5
2	OBS	27	0300	3.6	1.07	3.7	3.6	3.78	9.4	8.2	21.1	3.8
2	BDA	27	0300	3.7	0.31	3.7	3.7	0.29	4.7			
3	OBS	28	0000	3.4	0.45	2.9	3.5	1.71	5.2	7.7	11.8	3.8
4	OBS	29	1500	3.9	1.42	4.0	3.9	5.89	8.7	8.4	16.8	3.6
4	BDA	29	1500	3.9								
5	OBS	31	2000	3.6	0.71	2.8	3.6	2.27	7.2	7.4	8.5	2.5

* LPZ = long-period vertical-component seismometer.

† LPH = long-period horizontal-component seismometer.

proximately 35 degrees of freedom and were smoothed by hamming. Thus there is a 90% probability that the true power density (P_t) is in the range $0.71P_c \leq P_t \leq 1.58P_c$, where P_c is the computed value.

Power spectrums for the OBS seismometers corresponding to samples 2, 3, and 4 are shown in Figure 7. The period of the main peak ranges from 3.7 to 4.0 sec. As expected, the power density of the horizontal component is much larger than that of the vertical component. The period associated with the peak and the corresponding rms amplitudes for all five samples are listed in Table 2. The rms values were derived from the power density spectrums by integrating the function over the bandwidth of the peak and taking the square root of the result.

No attempt was made to remove the Doppler-shift signal discussed earlier. Thus the two peaks which usually appear between 5 and 8 sec in each spectrum actually represent water-wave motion and not ground motion. Small-amplitude ground motion at these periods would be masked by the Doppler-shift signal. However, no peak occurs at these periods on the BDA records and, for this reason, it was not considered worth while to subtract the Doppler effect before analysis. Of course, the signal-to-noise ratio for the seismic signal is degraded in this period range.

A feature of interest is the appearance of a secondary peak at about 3.2 sec in four of the spectrums. This peak is usually too close to the main peak to be well resolved, but it is par-

ticularly well developed in the LPZ spectrum of May 27. This point will be discussed further below.

Power spectrums from the BDA and the OBS records are compared at the time of the first peak in microseism activity (sample 2) in Figure 8. At this time, the power density for ground motion at the OBS site is larger than that for the island by a factor of 10 for the vertical component and 100 for the horizontal component, but the periods of the main peaks are very nearly the same. It appears that we are dealing with the same source of microseisms on the island as on the ocean bottom but that the amplitudes are much larger at the water-sediment interface than on the island surface.

No peaks in the BDA spectrums appear at periods corresponding to the water-wave periods, nor is there any evidence of the split peak in these spectrums. The seas were relatively calm at the time of this sample. It is of interest, in this connection, to consider the microseism spectrums at Bermuda during a period of high seas such as are produced by a hurricane.

Hurricane Arlene passed directly over Bermuda during August 1963. The time history of microseisms produced at Bermuda by this hurricane will be discussed in detail in section 6. For the purposes of this discussion, we consider only the power spectrum of a 15-min sample of microseisms recorded by the SPZ seismometer at the Bermuda station 11 hours after the eye had passed over the island (Fig-

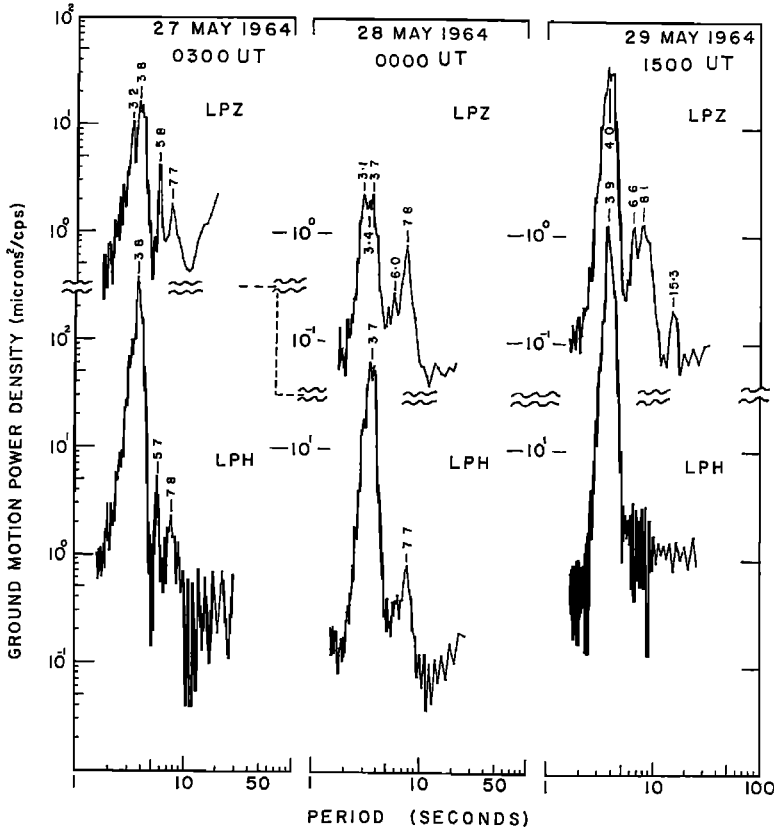


Fig. 7. Power spectrums of ocean-bottom microseisms for the LPZ and LPH seismographs. Note that the ordinate scale is not continuous between the upper and lower sections. The peaks near 6 and 8 sec correspond to water-wave motion, not ground motion. See text. All spectrums have been corrected for instrument response.

ure 9). The similarity between these two spectrums is evident, including the presence of the secondary peak in the island spectrum. It appears that if the storm is severe enough, measurable energy associated with the secondary peak does get into the island structure.

The short-period end of the spectrum is emphasized in Figure 10, where power spectrums are compared for the time of the first peak in microseismic activity (sample 2). The power density is consistently lower for BDA, by a factor of 10 at 1 cps, with some indication of a crossover point at higher frequencies where man-made and wind noise on the island might be expected to become dominant. There is no indication of a patterned spacing of peaks which could be associated with the 'organ pipe' modes reported by Bradner [1964].

It was pointed out above that the signal out-

put from the inoperative horizontal seismometer is due primarily to Doppler shift caused by the motion of the ship in response to wave action. Water-wave power spectrums obtained from this output are shown in Figure 11. The times of these three spectrums correspond to those of the ground-motion spectrums shown in Figure 7. The rms amplitudes for all five data samples are listed in Table 2.

The water-wave spectrum at 0300 UT, May 27, corresponds to the time of the first peak in microseismic activity and to the time of closest approach of the small low-pressure system to the southeast of the island. The sharp peak at 5.8 sec corresponds to a wind wave generated by this weather system. Greater power, however, is contained in the longer-period peak centered at 8.2 sec, which we will designate as 'swell' to distinguish it from the shorter-

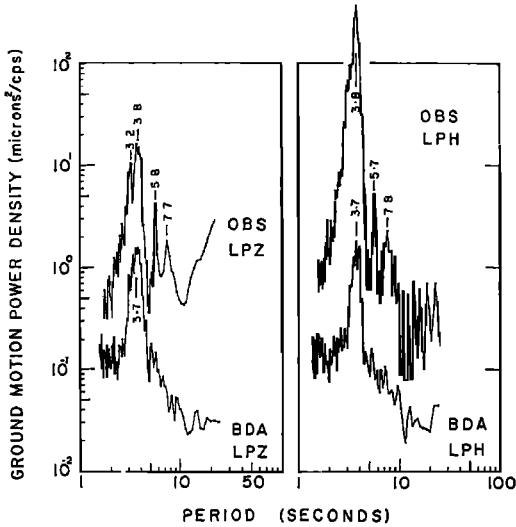


Fig. 8. Comparison between the power spectra of microseisms measured at the ocean-bottom site and the Bermuda standard station (May 27, 1964, at 0300 UT). Note that OBS peaks near 6 and 8 sec are related to water-wave motion, not ground motion. See text. Samples correspond to the time of the first peak in microseismic activity (sample 2). All spectrums have been corrected for instrument response.

period component. Swell components at longer periods also appear. This pattern repeats itself in all five water-wave power spectrums with minor variations in the periods of the various components. The period of the predominant peak is always near 8 sec.

The length of the receiving ship is equal to the wavelength of a water wave with a period of about 5 sec. Thus, if the long axis of the ship is perpendicular to the water-wave wavefronts, ship motion with periods of the order of 5 sec and shorter would be attenuated. However, the ship was hove to during most of the recording period, so that it tended to align parallel to the wavefronts. Thus the width of the receiving ship becomes the important factor. If we can ignore spurious motions resulting from ship resonances, the motion of the ship should follow water-wave motion for periods longer than 2 to 3 sec. Fortunately, independent wave measurements are available for comparison, so that a quantitative assessment of the importance of these factors is possible. The Oceanographic Prediction Division of the U. S. Naval Oceanographic Office has

installed an electronic wave staff at Argus Island, about 48 km north of the OBS site. This instrument has been described in detail by *Pickett* [1964]. Wave measurements from this installation made during the OBS experiment were kindly made available to us by J. Schule, Jr. (personal communication, 1964), before publication. The period of the main peak and the rms amplitudes of the waves from the Navy data are plotted in Figure 12, along with values from the five Doppler-shift spectrums computed in this study. The agreement between the two methods of measurement is quite good.

The two peaks in wave activity are concurrent with the peaks in microseismic activity; however, note that the second peak in water-wave amplitudes is smaller than the first, which is just the reverse of the microseism history. There appears to be no simple relation between water-wave amplitude and microseism amplitude at Bermuda. *Dinger and Fisher* [1955] reached the same conclusion in their study of microseisms at Guam. They concluded

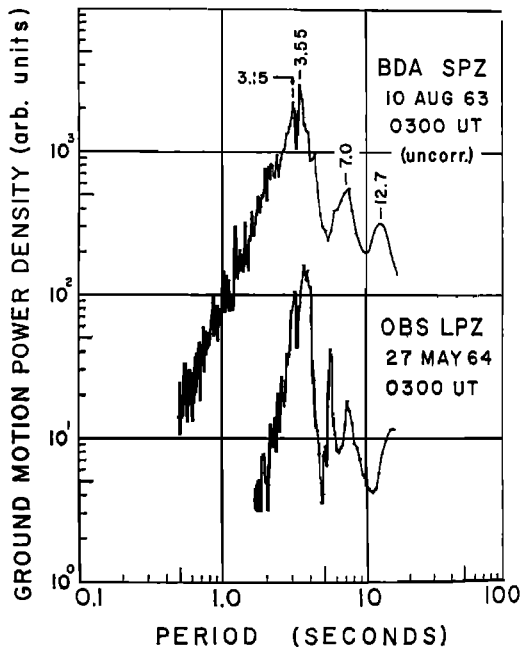


Fig. 9. Spectrums of microseisms recorded at Bermuda and on the ocean bottom. Both spectrums show the characteristic 'split peak'. The OBS spectrum (also in Figure 8) has been corrected for instrument response; the Bermuda spectrum is uncorrected.

that the largest microseism amplitudes occurred on the island when swell of about equal period approached the island from opposite sides. The measured wave periods were approximately twice the microseism periods. In a related study, *Dinger* [1963] compared power spectrums of water waves incident on the coast of Barbados with power spectrums of microseisms on the island. The periods corresponding to maximum microseism power density were again approximately one-half those of the corresponding maximum water-wave power densities. These results suggest that nonlinear interaction between opposing swells, in the manner described by *Longuet-Higgins* [1950], is the mechanism for microseism generation.

The periods of microseisms at the OBS site are compared with one-half the period of swell in Figure 13. These results were obtained from the power density spectrums and thus represent averages over 30-min samples. The curves remain nearly parallel to one another despite the small changes in period represented, but the microseism period is consistently less than one-half the swell period.

The shorter-period (wind-wave) peak in the wave spectrum remained near 6 sec during this experiment, and the period of the secondary peak in the microseism spectrums varied between 3.0 and 3.2 sec. This nearly 1/2 : 1 period relationship suggests that this secondary peak in the microseism spectrum might be related to

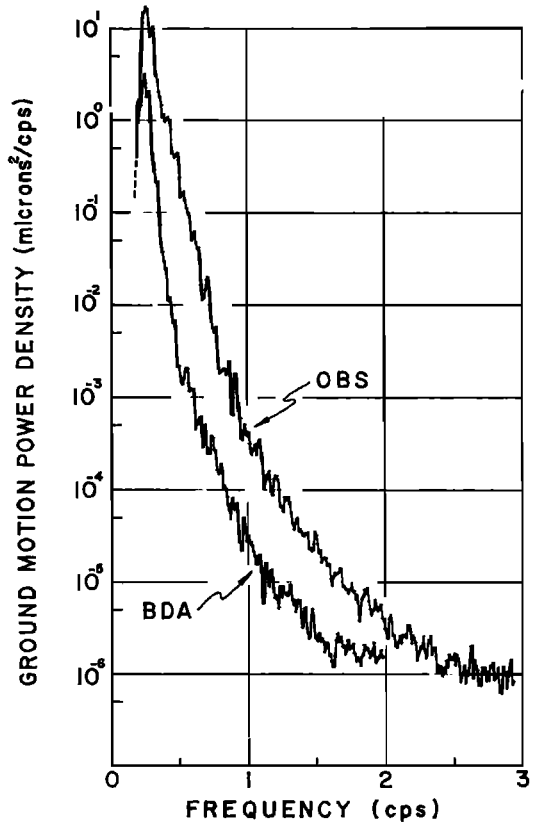


Fig. 10. Comparison between the high-frequency characteristics of power spectrums measured on Bermuda and on the ocean bottom (May 27, 1964, 0300 UT). Both spectrums have been corrected for instrument response.

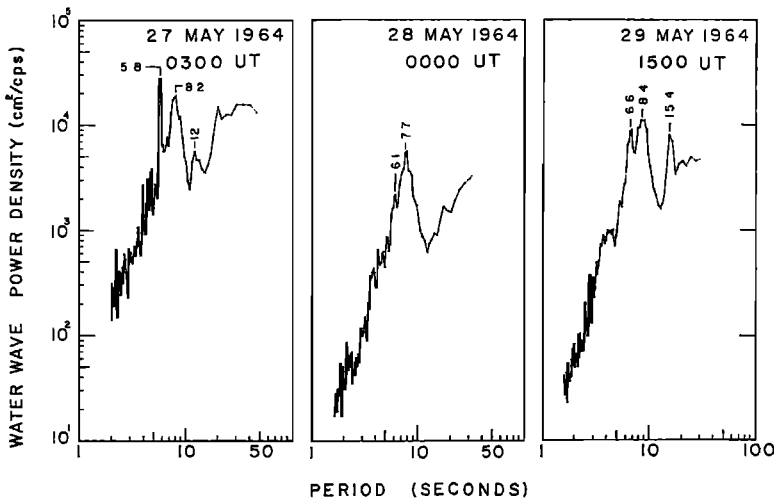


Fig. 11. Power spectrums of water waves measured above the OBS site as derived from Doppler-shift measurements.

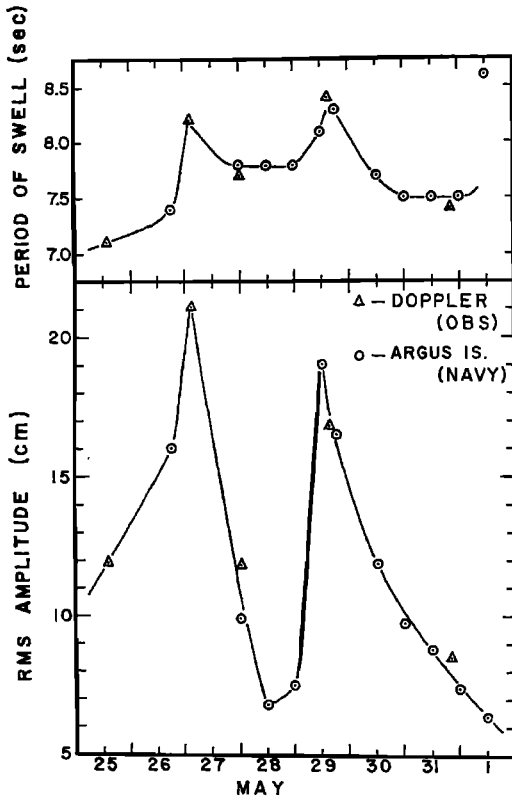


Fig. 12. Comparison between the period and amplitude of water waves as derived from (1) Doppler shift in telemetry signal and (2) an electronic wave-staff at Argus Island.

the wind-wave component of the water-wave spectrum in the same way that the primary microseism peak is related to swell.

Weather conditions do not appear to have favored the production of opposing swells at Bermuda during this study; hence we are inclined to favor the hypothesis that the interaction takes place between incoming waves and waves reflected back from the coast. In this case, the reflecting properties of the coastline facing the direction of incoming waves is a controlling factor in the resulting microseismic amplitudes. This implies that the northwestern and northern parts of the Bermuda coastline are better wave reflectors than the southern and southeastern parts of the island.

One qualifying point should be made—the sheltering effect of the island may have had some effect in reducing the peak water-wave amplitudes from the second storm. However,

the OBS site is far enough south of the island so that a substantial reduction in amplitudes caused by the island seems unlikely.

5. MODE OF PROPAGATION AND ENERGY

Measurements on land [Toksöz, 1964; Douze, 1964] indicate that most of the energy associated with microseisms propagating across land masses is in the form of fundamental and higher-mode Rayleigh waves. Measurements of microseisms directly on the ocean bottom have been reported by Ewing and Ewing [1961]; Monakhov [1962]; Prentiss and Ewing [1963]; Bradner and Dodds [1964]; Schneider and Backus [1964]; Schneider [1964]; Schneider et al. [1964]; and Bradner et al. [1965]. The only direct evidence bearing on the mode of propagation is given in the last four papers. Schneider and co-workers used a hydrophone in conjunction with a three-component short-period seismometer system. It can be shown [Biot, 1952] that the phase angle between pressure and vertical particle velocity is 90° for a free-traveling Rayleigh wave and is independent of frequency. The computations of cross-power spectrums reported by Schneider show a phase shift of $90^\circ \pm 10^\circ$ from the long-period end of the spectrum to a period of 0.5 sec. The sample described by Schneider was recorded 50 km west of Hawaii. The predominant period of the microseisms at the time was 4 sec. Thus the example makes a good comparison with the OBS results in both distance from the island and in the spectrum of the microseisms.

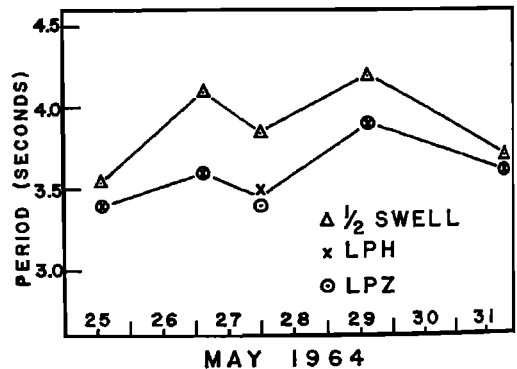


Fig. 13. Comparison between the period of the primary peak in microseism energy and one-half of the period of peak water-wave energy.

First results from the Lamont OBS system, located 170 km off the coast of northern California, corroborate the phase-shift observation. The predominant period of microseisms measured at this site on April 24, 1965, was 7.2 sec. Pressure leads vertical particle velocity by 90° , as predicted for Rayleigh waves, and the phase relation is consistent, so that the phase angle can be read on the seismograms without resort to cross-power computations.

We will present evidence in section 6 which suggests that the microseisms observed during this study were generated near Bermuda. Since the OBS is only 65 km south of Bermuda, it would have been quite close to the generating region where waves associated with leaky mode propagation might be expected to represent a significant contribution to the total seismogram. In particular, *Phinney* [1961], in his study of the oceanic *PL* mode, suggested that the late-arriving leaky modes (or organ-pipe modes) might be involved in the propagation of microseismic energy. However, it can be shown that the pressure and vertical particle velocity would be in phase for these modes. The phase angle would also be zero, or very close to zero, for the period range associated with the main energy from the other *PL* modes. Thus the observed 90° phase shift would appear to negate the importance of this mode of microseism propagation for periods longer than 1 sec. Since pressure was not measured during the Bermuda ocean-bottom experiment, this test cannot be applied in the present case.

Bradner et al [1965] used three-component seismographs for short-term measurements on the floor of the Pacific Ocean. They attempted to identify the wave types associated with propagation of microseisms by means of the phase relations and coherence between all three components of ground motion. For the most part, coherence was so low that this method failed. Where definite results were obtained, the wave type was identified as Rayleigh in two cases and Love in one case.

New data recorded during the Bermuda experiment bring one primary line of evidence to bear on the question of whether microseisms propagate in normal modes: the ratio of horizontal-to-vertical particle motion (Rayleigh constant). The measured value for this

ratio was quite stable for the ocean-bottom data, with an average value of 3.5. The theoretical ratios of horizontal-to-vertical particle motion at the top of the sediments are plotted as a function of period for the Rayleigh mode and the first and second shear modes in Figure 14. The experimental points are the ratios of the rms amplitudes listed in Table 2. In this period range the fundamental mode particle motion is prograde and the ratio u/w is relatively constant in comparison with the steep gradients observed in the curves for the first and second shear modes. Although they cover only a narrow part of the period range, the experimental points fit the fundamental mode ratio quite well.

The ratio of u/w for the secondary peak (between 3.0 and 3.2 sec) in the microseism spectrum is not as well defined, but it is approximately 2.2. The theoretical ratio values for the oceanic model (4-B) at 3.1 sec are 2.5,

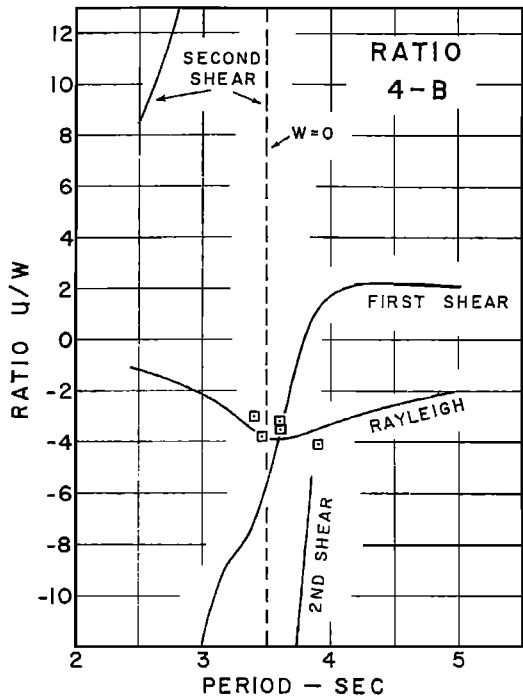


Fig. 14. Theoretical ratio of horizontal-to-vertical particle motion at the top of the sediment layer for the first three Rayleigh modes (model 4-B). Positive ratio indicates retrograde motion; negative ratio indicates prograde motion. Five experimental points are plotted for comparison.

9.9, and 24.2 for the fundamental mode, first shear mode, and second shear mode, respectively. Hence it appears likely that microseisms related to this peak are also Rayleigh waves of the fundamental mode. The approximately $\frac{1}{2} : 1$ period relation to wind waves suggests that the shorter-period microseisms are generated by the wind-wave component of the water-wave spectrum in the same way that the longer-period microseisms are generated by the swell component.

The effects of changes in model parameters on the ratio curves for the first and second shear modes are shown in Figures 15 and 16. Small changes in model parameters produce large changes in the ratio curves for these modes. The change from model 4-B to 5-B is a thickening of the sediment layer from 0.31 to 0.50 km. Variations in sediment thickness of this order are certainly present in the vicinity

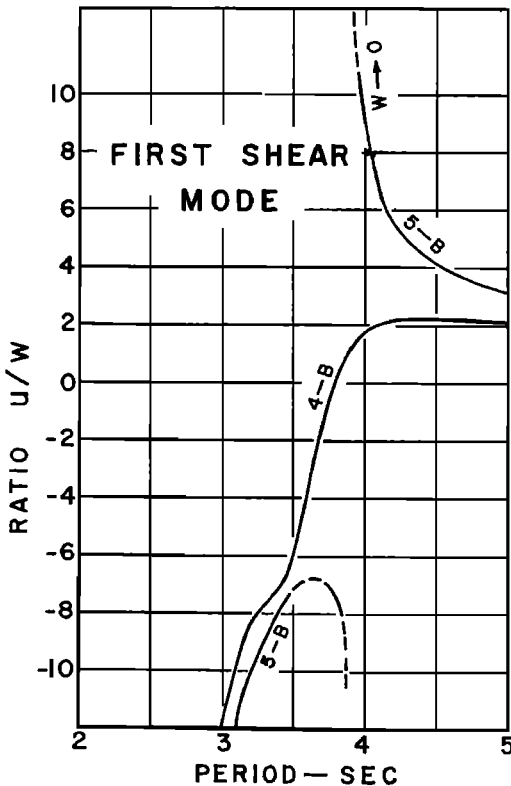


Fig. 15. Theoretical ratio of horizontal-to-vertical particle motion at the top of the sediment layer for the first shear mode (models 4-B and 5-B). Positive ratio indicates retrograde motion. Negative ratio indicates prograde motion.

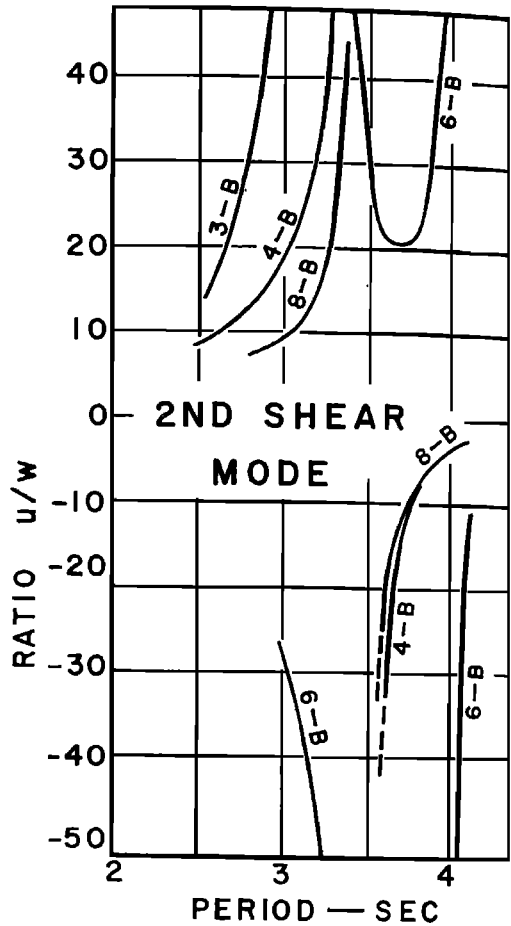


Fig. 16. Theoretical ratio of horizontal-to-vertical particle motion at the top of the sediment layer for the second shear mode (models 3-B, 4-B, 6-B and 8-B). Positive ratio indicates retrograde motion. Negative ratio indicates prograde motion.

of Bermuda [Ewing and Ewing, 1963]. Model 3-B represents the removal of 10 meters from the top of the sediment layer. Model 6-B represents a thickening of the water layer from 4.4 to 5.0 km. Model 8-B represents a change in thickness of the basement layer from 1.3 to 2.3 km. In the range of periods corresponding to large microseisms, all the ratio curves for the higher modes have steep gradients. These various models, and others which are not shown, were tried in an attempt to find one that would bring the ratio value for one of the higher modes into closer harmony with the experimental points. No models were found which

were reasonably close to the local structure determined from seismic measurements and for which the ratio curves fit the experimental points.

The fundamental mode is affected largely by the sediment layer, or, more precisely, by the top part of the sediment layer at these short periods. Other changes in the model, such as water depth or basement thickness, have little effect on the ratio.

The observed ratio on Bermuda is approximately 1. The theoretical ratios (model 7-B) at 3.7 sec period are 0.72 for the fundamental mode, 0.57 for the first shear mode, and 0.26 for the second shear mode. Thus the observed u/w ratio supports the fundamental mode as the most likely mode of propagation of microseisms at both the OBS and BDA sites.

It should be recognized that the theoretical

ratio applies to a single wavetrain, whereas it is possible that the microseisms at a given point consist of the superposition of Rayleigh waves arriving continuously from many directions. A distributed source would produce the low coherence observed between the horizontal and vertical components [Schneider, 1964] and might modify to some extent the ratio of horizontal-to-vertical motion [Strobach, 1965]. We next consider some of the pertinent aspects of short-period Rayleigh wave propagation in the oceanic structure.

The horizontal and vertical particle-motion profiles associated with the Rayleigh mode and the first and second shear modes are shown in Figure 17. For the OBS site (4-B), the Rayleigh mode computation was repeated with the sediment layer removed (lower curves) to show the profound effect of a thin layer of sediment

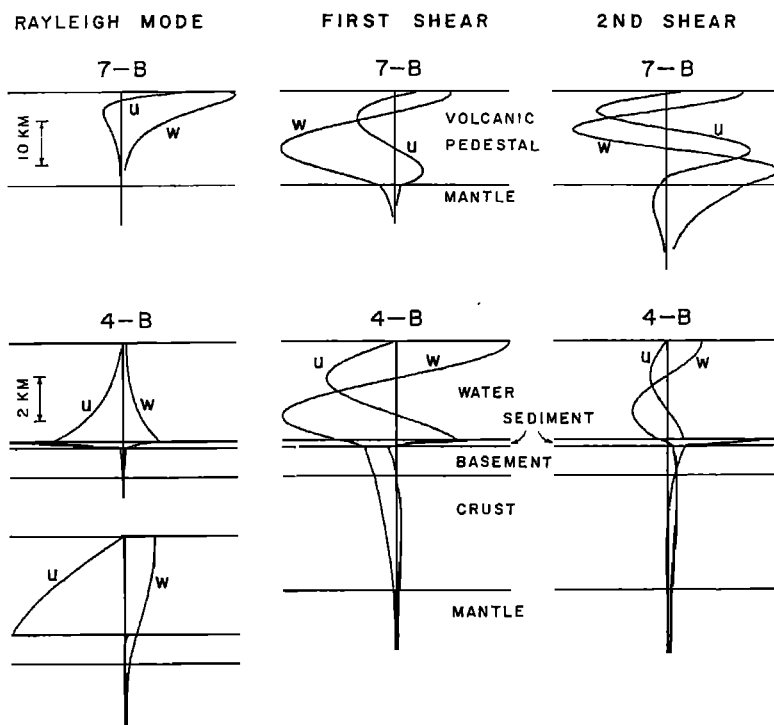


Fig. 17. Theoretical particle-motion profiles corresponding to the first three Rayleigh modes for the Bermuda pedestal model (7-B), and the oceanic model (4-B). u , w denote horizontal (longitudinal) and vertical motion, respectively. The period is 3.7 sec in all cases. The two sets of curves shown for the Rayleigh mode, model 4-B, correspond to the case with sediment (upper curves) and without sediment (lower curves). Like signs on u and w indicate retrograde motion; opposite signs indicate prograde motion. Note that the vertical scale is five times larger for the oceanic model than for the Bermuda pedestal model.

(0.31 km) at these short periods. When no sediment is present, the profile shows relatively small retrograde motion at the top of the solid. With the addition of a thin sediment layer, maximum particle amplitudes occur at the liquid-solid boundary instead of at the free surface; the horizontal motion in the sediments just beneath the interface becomes much larger relative to the vertical motion, the Rayleigh constant increasing from 0.33 to 3.9; and the motion at the top of the sediments becomes prograde. The energy becomes progressively more concentrated in the sediment layer for shorter periods (or thicker sediments).

Figure 17 shows that at a period of 3.7 sec the water-sediment interface is an antinode for both horizontal and vertical motion for the fundamental mode. *Press and Ewing* [1948] point out that vibration in an acoustical system is excited most efficiently by applying the driving force at an antinode. Following this line of reasoning, we see that the proper place to apply a force in the oceanic acoustical system to produce Rayleigh wave motion in the fundamental mode, for the period range of the observed microseisms, is at the water-sediment interface. Assuming that the excitation derives from a force applied at the surface of the water layer, we would therefore expect that generation would not take place very efficiently in deep water over unconsolidated sediments. Unconsolidated sediments pinch out against the flanks of Bermuda at a depth of approximately 4 km. In shallow water the vertical particle motion antinode is at the water surface, and this favors generation by a surface source. Therefore, if the observed microseisms are fundamental mode Rayleigh waves, generation probably takes place near Bermuda. The validity of this suggestion is strengthened by other evidence in section 6. These arguments do not hold in relation to the generation of microseisms with a period so long that the antinode would be at the surface even in the presence of unconsolidated sediments.

To obtain the actual amplitudes of the various Rayleigh modes as a function of period, the excitation functions must be computed. The form of the excitation function will depend on the assumed model, i.e., on the roots of the period equation, on the location of the receiver, and on the nature and location of the source. In

their investigations of the problem, *Scholte* [1943] and *Press and Ewing* [1948] consider a point source of pressure at the surface. *Longuet-Higgins* [1950] expanded on this theory by considering a distribution of point sources. *Hasselmann* [1963] has departed from the concept of discrete, harmonic point sources and considers the excitation to be due to a randomly distributed pressure field. All these authors recognized the important concept that the amplitude spectrum of the normal mode excitation of the system depends on both the acoustical response, or system transfer function, and on the source spectrum. For the purposes of this paper, the influence of the layered medium will be investigated in the following way: We assume nothing about the nature of the source function and accept only the fact that the source does put energy into the waveguide which radiates away from the generating region as Rayleigh waves. A simple energy argument can then be used to determine at what period maximum amplitudes can be expected on the ocean bottom.

Rayleigh [1894] demonstrated the following relation for a propagating surface wave

$$\bar{F} = U\bar{E} \quad (3)$$

where

\bar{F} = energy flux, the average energy per unit time passing through a vertical plane surface of unit width and infinite depth, perpendicular to the direction of propagation.

\bar{E} = energy density, the mean total energy averaged over one wavelength, contained in a vertical column of infinite depth and unit area.

U = group velocity.

Biot [1957] demonstrated the validity of (3) under very general conditions, and *Tolstoy* [1955, 1956] employed this concept in the direct computation of group velocity. If the elastic system is conservative, energy flux radiated away from the source must equal the power supplied by the source. Thus, if \bar{F} is interpreted as source power, the input power required to maintain a given energy density in the outgoing wavefront at a given period is given by (3). To be meaningful in this case, the energy density values must be adjusted at each period so that the corresponding particle motion amplitude at the point of meas-

urement is held constant. For the present case, the point of measurement is just beneath the water-sediment interface. Energy density values normalized in this way are designated \bar{E}_n . A minimum value in a plot of normalized energy density versus period corresponds to the period at which minimum system energy is associated with a given amplitude at the point of measurement. Then, by (3) and the foregoing arguments, the minimum source power required to sustain Raleigh wave motion at given amplitude and distance is given by the minimum value of the quantity $U\bar{E}_n$. To separate source effects from transmission effects, we assume that the spectrum of the energy actually coupled into the waveguide is flat (white). The largest amplitudes will then be associated with the period range for which the energy flux is a minimum. We proceed to the computation of \bar{E}_n .

Energy density can be expressed as

$$\bar{E} = \frac{1}{\lambda} \int_0^{\lambda} dx \int_{-\infty}^{+\infty} \rho(\dot{u}^2 + \dot{w}^2) dZ \quad (4)$$

where ρ , \dot{u} , and \dot{w} are the density, horizontal particle velocity, and vertical particle velocity, respectively, all of which are functions of depth Z . The horizontal wavelength is λ . For a single sinusoidal wavetrain, the particle velocities squared introduce x -dependent terms $\sin^2k(x - ct)$ and $\cos^2k(x - ct)$. The value of either term averaged over one wavelength is $1/2$. Hence (4) simplifies to

$$\bar{E} = \frac{1}{2} \int_{-\infty}^{+\infty} \rho \omega^2 (u^2 + w^2) dZ \quad (5)$$

u and w are given as functions of depth in particle-motion profiles of the type discussed above. Thus the energy density associated with the propagation of a Raleigh wave can be computed by numerical integration of (5) from the surface to a depth where the particle motion becomes insignificant.

The values of U , \bar{E}_n , and \bar{F} corresponding to the fundamental mode Raleigh wave for the oceanic structure are plotted in Figure 18. The energy flux, energy density, and group velocity all show a minimum at approximately 3.3 sec. It is at this period that we would expect maximum amplitudes in the steady state if (1) the chosen model for the OBS site is correct and (2) the spectrum of the energy actually coupled into the waveguide is flat.

The predominant period of microseisms observed on the ocean bottom varied between 3.4 and 3.9 sec. However, the period of microseisms at Bermuda was not significantly different from that measured concurrently at the OBS site. If the zone of generation of microseisms is primarily on the flanks of the island, as we contend in section 6, the propagation path was through the island structure to the Bermuda seismograph station in the first case and primarily through the oceanic structure to the OBS site in the second case. Since the properties of these two paths are certainly different, the layered medium would not appear to have greatly influenced the observed microseism periods. Assuming that gravity waves are, directly or indirectly, the most likely source, this result suggests that the water-wave spectrum normally represents a very narrow band source relative to a function which correctly describes the response of the layered medium; thus the water-wave spectrum will usually be

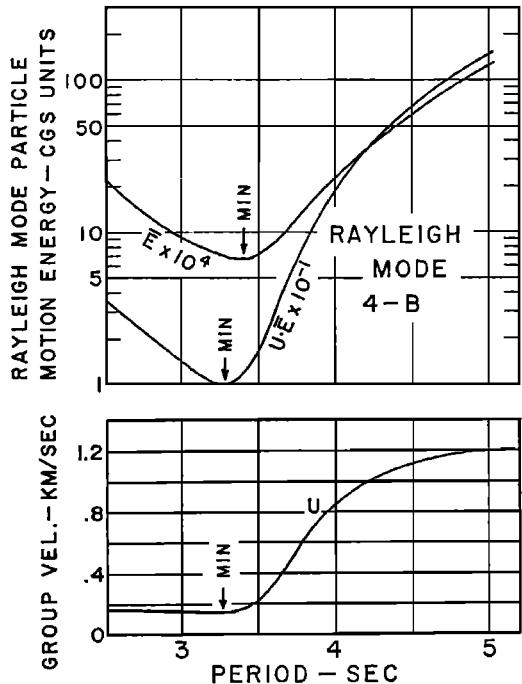


Fig. 18. Energy density and energy flux associated with a fundamental mode Raleigh wave for ocean-bottom model 4-B. The numerical values correspond to $u = 0.707 \mu$ at the top of sediment layer. Group velocity for fundamental mode Raleigh waves, model 4-B.

the dominant factor in shaping the microseism spectrum. It is only when the source is relatively broad band, such as might be produced by a hurricane at close range, that the influence of the layered medium becomes important.

While on the subject of energy, it is of interest to compare the energy flux of microseisms at OBS with that at BDA. Before performing this computation, we scaled the theoretical particle-motion profiles so that the amplitudes at the island surface (model 7-B) and at the top of the sediments (model 4-B) agreed with the averages of the measured values. The resulting values of u/w agree well with the theoretical values for the first mode only. The mean energy density and mean energy flux associated with these adjusted particle-motion curves for the Rayleigh mode and the first and second shear modes are listed in Table 3. The period in all cases is 3.7 sec.

In Table 3, two points are of particular interest: (1) the energy flux is about the same for the island and ocean-bottom structures if either fundamental mode or second shear mode propagation is assumed and is 2.5 times larger at the island site if first shear mode propagation is assumed; (2) the energy flux generally increases with mode number. With reference to the second point, consider, e.g., the ocean-bottom case (4-B). If power P_0 must be delivered into the waveguide to sustain a given

particle-motion amplitude at the water-sediment interface at an arbitrary distance from the source when the energy radiates outward in the fundamental mode, then power $P_1 = 5P_0$ is required if the transmission is in the first shear mode, and $P_2 = 15.3P_0$ is the required source power if second shear mode propagation is assumed. Thus transmission in the fundamental mode requires considerably less source power than for the higher modes. In this argument, variations in distance-dependent attenuation among the modes are ignored.

With reference to water waves as a possible source of energy for the generation of microseisms, it is of interest to compare the energy flux transported by water waves impinging on the coast with the energy flux present in the microseism field.

The energy flux of water waves in deep water is given by

$$F_w = g\rho H^2 U \quad (6)$$

where $U = gT/4\pi$ is the group velocity of water waves, H the rms wave amplitude, g the gravity field strength, ρ the density of water, and T the wave period.

Typical values measured in this study are $H = 20$ cm and $T = 8$ sec, which gives $F_w = 2.4 \times 10^8$ ergs/cm sec. For microseisms at the OBS site, a vertical particle-motion amplitude of 1.6μ and a period of 3.7 sec are representative values. Using these values and assuming

TABLE 3. Energy Density and Energy Flux Associated with Passage of a Rayleigh Wave of 3.7 Seconds Period through the Island Structure and the Oceanic Structure

Site	Model	Mode	Experimental* Rayleigh Constant	Theoretical Rayleigh Constant	Mean Energy Density, ergs/cm ² $\times 10^{-6}$	Group Velocity, cm/sec $\times 10^{-6}$	Mean Energy Flux, ergs/cm sec $\times 10^{-3}$
OBS	4-B	0	3.9	-3.84	16.75	0.49	1.03
BDA	7-B	0	1.2	+0.72	4.43	2.72	1.50
OBS	4-B	1	3.9	-1.41	45.05	0.89	5.02
BDA	7-B	1	1.2	+0.57	37.84	2.71	12.9
OBS	4-B	2	3.9	-13.6	163.03	0.77	15.7
BDA	7-B	2	1.2	+0.26	37.59	2.70	12.8

* The theoretical particle-motion profiles were adjusted so that $Z(\text{BDA}) = 1.0 \mu$; $H(\text{BDA}) = 1.2 \mu$, $Z(\text{OBS}) = 3.2 \mu$, $H(\text{OBS}) = 12.5 \mu$, where Z and H refer respectively to the amplitudes (peak to peak) of the vertical and horizontal components of ground motion. These amplitudes correspond to the averages of the measured values.

fundamental mode propagation, we get a microseismic energy flux in the oceanic structure of 1.0×10^3 ergs/cm sec. Thus the energy flux associated with water waves incident on Bermuda is approximately 10^5 times larger than that of microseisms propagating past the OBS site.

We conclude that (1) the observed ratios of horizontal-to-vertical particle motion at the OBS and BDA sites fit the theoretical values for Rayleigh waves of the fundamental mode; (2) if the microseisms are Rayleigh waves of the fundamental mode, approximately the same energy flux is associated with microseisms propagating in the oceanic structure as in the island structure; and (3) water waves incident on Bermuda are potentially the energy source for the observed microseisms. Also, we are now able to explain that the ocean bottom is a noisy recording site relative to the surface of Bermuda. As shown above, the energy flux is approximately the same at both sites. The larger amplitudes recorded on the ocean bottom result primarily from the difference in the distribution of energy with depth at the two sites. In the presence of unconsolidated sediments the energy associated with a short-period (≈ 4 sec) Rayleigh wave propagating through the oceanic structure in the fundamental mode is concentrated near the water-sediment interface, i.e., at the recording depth. No such concentration of energy occurs at the island surface. If no sediments were present at the OBS site, the amplitudes of microseisms would have been smaller by a factor of approximately 8 for the vertical component and 94 for the horizontal component. In the absence of sediment the ocean bottom would have been a quieter recording site than the Bermuda station by a factor of approximately 3 for the vertical component and 9 for the horizontal component. These are computed values which depend on the characteristics of the chosen models (4-B, 7-B) but the validity of the argument depends only on the presence of an appreciable thickness of unconsolidated sediments on the ocean bottom.

6. LOCATION OF THE SOURCE REGION

The question of the location of the source region is fundamental to any theory on the generation of microseisms. The power spectrums of microseisms generated on Bermuda

by Hurricane Arlene, in August 1963, were discussed in section 4. For the purposes of the present discussion, it is instructive to examine the history of the microseisms produced by this hurricane. The amplitude and period of the dominant microseisms on seismograms recorded at the Bermuda standard station (LPZ) were measured every 2 hours. The measured values are shown in Figure 19. *Carder* [1955] studied microseisms at Bermuda associated with the passage of thirteen hurricanes in the western North Atlantic. The following features are characteristic of the hurricane microseisms related to Arlene and those studied by *Carder*: (1) there is a very small increase in amplitude in the period range of 4 to 6 sec as the storm approaches the island; (2) as the central winds pass off the northern side of the island, a very rapid increase in amplitude occurs and the period shortens to about 4 sec; and (3) as the hurricane moves away from the island, microseism amplitudes slowly decay and the period remains at about 4 sec.

It is very difficult to reconcile these observations with a theory that includes generation of microseisms directly beneath the storm, although they are easily explained in terms of generation by wave action near Bermuda. Consider first the asymmetry of the amplitude variation. Maximum winds had actually passed off the northern edge of the island before microseism amplitudes reached their maximum values. This would certainly not be expected if microseisms were being generated beneath the storm as it approached the island. The shape of the amplitude curve is, in fact, just about what would be expected for water waves arriving from a fast-moving storm. The storm neared the island with a velocity of about 35 to 40 km/hr. This is equal to the group velocity for water waves of 13 sec period. Hence, only waves with periods longer than 13 sec could propagate ahead of the storm. Such waves would have relatively low amplitudes. This would account for the longer period and low amplitudes associated with the onset of increased microseismic activity. When the area of high winds and high wave activity arrives at the island, the microseism amplitudes increase rapidly to their peak and remain high in the wake of the storm, just as wave activity in the vicinity of the island would. The water-wave spectrum for the storm

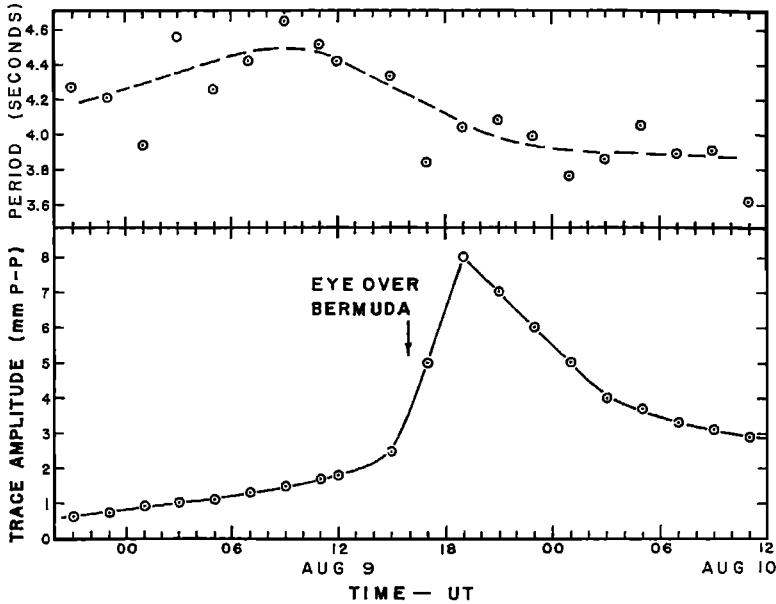


Fig. 19. Period and amplitude of microseisms measured on the island of Bermuda during passage of Hurricane Arlene, August 1963.

area itself is certainly peaked at a shorter period than the preceding storm swell; thus, if water waves near Bermuda produce the microseisms observed on the island, a decrease in the period of microseisms as a hurricane strikes the island is to be expected. The area of generation for microseisms must therefore be very near the island. *Dinger* [1963] reached the same conclusion from his study of microseisms and water waves on the island of Barbados.

The similarity of the Q values for the spectral peaks of concurrent water waves and microseisms is further evidence for a cause-and-effect relationship between local water waves and microseisms. Q was obtained from the power density spectrums by measuring the frequency corresponding to the pertinent peak and dividing by the bandwidth at the half-power points. The average Q in Table 2 is 3.4 for the vertical component of the OBS and water waves and 7.2 for the horizontal component of the OBS. Q values are expected to be larger for the horizontal component than for the vertical component of motion because, for the fundamental mode, the ratio of horizontal-to-vertical motion has a maximum in the period range of the spectral peaks (see Figure 14). *Haubrich et al.* [1963] obtained $Q \approx 14$ for both micro-

seisms and water waves from distant storms. The Q values measured in this study are much smaller than those reported by *Haubrich* because we are dealing with comparatively nearby storm systems. However, in both studies the Q for microseisms is approximately equal to the Q for water waves, despite the large contrast in the range of Q values between the two studies.

No consistent phase relation between the horizontal and vertical components can be seen on the OBS records, so that the direction of propagation of the microseisms cannot be determined without using some type of time averaging process. The same is true of the standard station seismograms at Bermuda. For this purpose an analog method essentially as described by *White* [1964] was used.

For a Rayleigh wave of period $2\pi/\omega$ the horizontal and vertical particle motion at a fixed point can be expressed by

$$H = A \cos \theta \cos \omega t \quad (7)$$

$$Z = (A/K) \sin \omega t \quad (8)$$

where K is the ratio of horizontal-to-vertical particle amplitude and θ is the angle between the surface-wave ray path and the sensitive axis of the horizontal seismometer.

Written in this form, H leads Z by 90° . This would be true for a wave with prograde motion from the northeastern sector or for a wave with retrograde motion from the southwestern sector. It will be shown in section 7 that the 'up' direction on the horizontal-component seismograph represents particle motion to the northeast (azimuth = 38°); hence the northeastern sector spans the semicircular arc from 52° west of north to 128° east of north and the southwestern sector includes the opposite 180° span. Consider the quantities

$$I_1 = \langle HZ \rangle / (\langle H^2 \rangle \langle Z^2 \rangle)^{1/2}$$

$$I_2 = \langle H\dot{Z} \rangle / (\langle H^2 \rangle \langle \dot{Z}^2 \rangle)^{1/2}$$

where the angle brackets indicate the time average of the quantity within the brackets over some specified time interval.

Substituting for H and Z from (7) and (8), we see that $I_1 = 0$ and $I_2 = 1$ for a Rayleigh wave. It follows that the time integral of I_1 is zero, and the integral of I_2 will increase linearly with time. Similarly, if Z leads H by 90° , $I_1 = 0$, $I_2 = -1$, and the integral of I_2 will increase in the negative direction. If, instead of a unidirectional source, microseisms arrive at the detector with equal energy from all directions, but with random phases, all these quantities will be zero. This result follows from the same arguments used in showing that the cross power between horizontal and vertical particle motion is zero for a perfectly isotropic source. See White [1964] for the details of the argument. A perfectly isotropic field is as improbable as a perfectly unidirectional field. Hence we do not expect these quantities to be precisely 0 or 1.

The quantities I_1 and I_2 and their integrals were formed by analog means from magnetic-tape playback. An example of the resulting output signal, along with the sample of microseisms fed into the signal processor, is shown in Figure 20. Averaging in this case was done with a low-pass filter (time constant 20 sec); hence we have, in effect, a running average over about 5 cycles of the signal. The value of I_2 definitely tends toward $+1$, as is confirmed by the integral, whereas I_1 appears to average near zero for the sample as a whole. The polarities are such that $I_2 = +1$ indicates that energy comes predominantly from the northeastern sector if the particle motion is prograde, i.e., the energy

comes predominantly from the direction of the island and not from the seaward side of the OBS. A selection of samples was analyzed throughout the recording period and all samples showed this same relationship. Specifically, this result was obtained during the first peak in microseismic activity when the associated weather system was located south of the OBS site. Thus the directional study supports the conclusion that the 4-sec microseisms are generated primarily in the immediate vicinity of the island.

Some of the irregularity in the quantities I_1 and I_2 may be caused by the presence of higher-mode particle motion which may be retrograde or prograde in this period range. The opposite direction is indicated if the particle motion is retrograde. However, if the energy propagates in the Rayleigh mode, the motion is prograde at these short periods for any of the models discussed in this paper. It appears that Bradner *et al.* [1965] failed to recognize the possibility of prograde particle motion in their study of microseisms recorded on the ocean bottom in the Pacific. Their conclusions regarding the probable source regions for microseisms of intermediate period (≈ 6 sec) are based on the assumption that the Rayleigh wave particle motion is retrograde. In the specific case in which hodographs of microseismic particle motion are shown, Bradner *et al.* suggest that a storm located north of the recording site might be the source. If the particle motion is actually

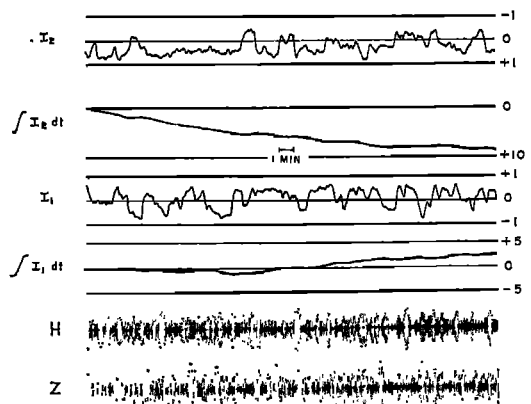


Fig. 20. Sample of ocean-bottom microseisms (recorded May 29, 1964, at 1700 UT) and related quantities derived by means of an analog computer.

prograde, the direction of propagation is reversed from that given by Bradner et al., and the source region could be in the island chain (Samoa Islands) south of the recording site.

7. EARTHQUAKES

Phases from nine earthquakes have been identified on the OBS records. The data are

TABLE 4. Seismic Events Identified on Seismograms from the Ocean-Bottom Seismograph

Arrival times are corrected for travel time in the water layer (-3.0 sec).

Phase	Time, UT			Epicenter Data (USCGS)
	h	m	s	
South Sandwich Islands, May 26, 1964				
<i>iP</i>	11	12	18.5	10 59 12.3, $\Delta = 93.0^\circ$
<i>ePP</i>	11	16	04	56.2°S, 27.8°W
<i>iSKS</i>	11	22	40	$M = 7\frac{1}{2}$, $h = 120$ km
<i>eS</i>	11	23	01	
<i>eSS</i>	11	29	35	
<i>eLR</i>	11	41	50	
Dominican Republic, May 28, 1964				
<i>iP_{hf}</i>	01	30	57	01 27 49, $\Delta = 12.7^\circ$
<i>iS_{hf}</i>	01	33	04.1	19.6°N, 70.2°W
<i>eT_{max}</i>	01	44	19	$M = ?$, $h = 33$ km
Mid-Atlantic Ridge, May 28, 1964				
<i>eLR</i>	12	55	29	12 33 10.2 0.8°S, 24.7°W $M = 5.2$, $h = 33$ km
Dominican Republic, May 29, 1964				
<i>iP_{hf}</i>	00	22	55.8	Not reported by USCGS
<i>iS_{hf}</i>	00	24	59.1	
Alaska (aftershock), May 29, 1964				
<i>eLR</i>	10	42	42	10 17 34.5 60.2°N, 146.3°W $M = 5.6$, $h = 5$
Honshu, Japan, May 30, 1964				
<i>eLR</i>	15	23		14 30 45.3 36.2°N, 141.1°E $M = 5.5$, $h = 49$ km
Kurile Islands, May 31, 1964				
<i>eP</i>	00	56	12	00 40 36.4, $\Delta = 99.8^\circ$
<i>ePP</i>	01	00	18	43.5°N, 146.8°E
<i>eS</i>	01	05	32	$M = 6\frac{1}{2}$, $h = 48$ km
<i>eSS</i>	01	12	40	
<i>eLQ</i>	01	23	56	
<i>eLR</i>	01	27	48	
Dominican Republic, May 31, 1964				
<i>iP</i>	10	33	24.5	10 30 25.0, $\Delta = 13.1^\circ$
<i>iP_{hf}</i>	10	33	25.6	19.2°N, 69.4°W
<i>iS_{hf}</i>	10	35	33.3	$M = 5.0$, $h = 83$ km
Dominican Republic, May 31, 1964				
<i>iP_{hf}</i>	10	44	21.8	Not reported by USCGS
<i>iS_{hf}</i>	10	46	28	

listed in Table 4. Five additional high-frequency events were recorded. These were probably arrivals from distant explosions in the water, although it is possible that some of them are *T* phases. In the search for seismic events the signal-to-noise ratio was increased by playing the magnetic tape records back through band-pass filters. It is reasonably certain that other earthquake phases could be located by using better filtering techniques.

A series of four earthquakes having similar characteristics was recorded. Slow-speed recordings of all four events are shown in Figure 21. Only two of the earthquakes were located by the U. S. Coast and Geodetic Survey (see Table 4), but, considering their nearly identical *S-P* time intervals and similar appearance, they all

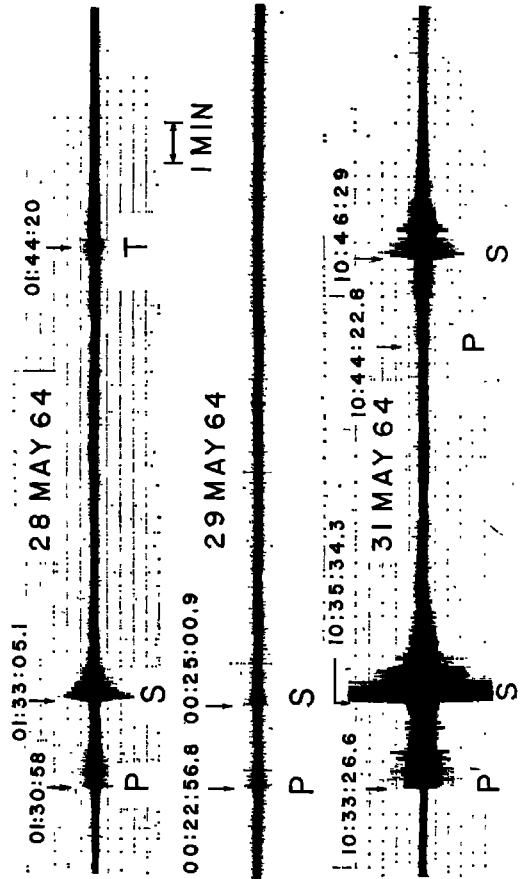


Fig. 21. Seismograms recorded on the ocean bottom showing high-frequency *P* and *S* phases from four small Dominican Republic earthquakes (see Table 4).

undoubtedly occurred in the same region near the north coast of the Dominican Republic, at a distance of about 13° from the OBS site. The most striking features of these seismograms are the high-frequency content of the P and S phases and their long duration. These characteristics of West Indies earthquakes have been described by *Linehan* [1940], *Leet et al.* [1951], *Shurbet* [1962], and *Isacks and Oliver* [1964]. A high-speed record of the largest Dominican Republic shock is shown in Figure 22. A section of the record was removed between the P and S phases to permit large-scale reproduction.

The high-frequency phases have maximum amplitudes between 10 and 11 cps. These arrivals have not been Fourier-analyzed to determine the possible presence of subordinate spectral peaks. There is no measurable difference in predominant frequency between the P and S phases. No dispersion is apparent in either the P or S wavetrain.

For the largest and best-recorded Dominican Republic earthquake we obtain velocities of 8.05 km/sec for the beginning of the P_{hr} phase and 4.71 km/sec for the beginning of the S_{hr} phase. These values are consistent with velocities derived for the upper mantle in the western North Atlantic from seismic refraction studies [*Katz and Ewing*, 1956]. The travel-time curves derived for P_{hr} and S_{hr} by *Shurbet* [1962] show a more linear trend than the Jeffreys-Bullen P and S travel-time curves. On the basis of the observed velocities and the linearity of the travel-time curves, it appears that the high-frequency phases can properly be called P_n and S_n . The predominant frequency in the high-frequency arrivals is very nearly the same for

all four earthquakes, whereas the maximum amplitudes from the smallest earthquake to the largest differ by an order of magnitude. It is difficult to believe that the source spectrums could have been so uniform for such a large variation of released energy. Thus the sharpness of the signal spectrum appears to be a propagation effect.

The arrival of the high-frequency phase, P_{hr} , in Figure 22 is preceded by a lower-frequency wavetrain (4 cps) which is identified as the normal P phase. The time interval between these two arrivals is 1.1 sec. For the largest earthquake, the high-frequency P phase is barely visible on the Bermuda standard station record (≈ 0.05 mm peak to peak) and the normal P wave arrival is not visible at all. The predominant frequency in the P_{hr} arrival at Bermuda is approximately 6 cps. The actual ground motion was 6 times larger on the ocean bottom than at the standard station on Bermuda.

The ground-motion amplitudes of various earthquake phases at the ocean-bottom site are compared with those at the Bermuda standard station in Table 5 (column 4). Only those phases which showed a close similarity in waveform between the two sites were used. The ground motion at short periods, as was mentioned above, is larger on the ocean bottom than at the surface of the Bermuda pedestal. The dominance of high-frequency signal on the ocean floor relative to nearby land stations has also been noted by the Texas Instruments group [*Schneider*, 1964]. They report that earthquake signal energy on the ocean bottom is greater than at nearby land stations by as

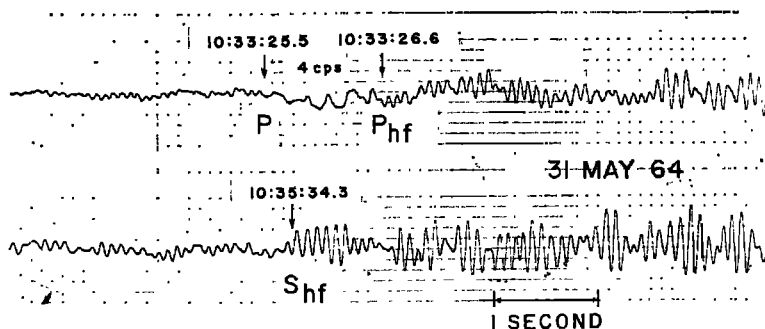


Fig. 22. High-speed recording of the P and S phases from a Dominican Republic earthquake (see Table 4).

TABLE 5. Comparison of Ground-Motion Amplitudes for the Ocean-Bottom Site and the Bermuda Standard Station

Component	Phase	Predominant Period, sec	BDA Microseisms†		Predominant Microseism Period	BDA <i>S/N</i> OBS <i>S/N</i>	
			BDA Signal* OBS Signal	OBS Microseisms			
Kurile earthquake	LPZ	<i>P</i>	14	2.5	0.39	3.8	6.4
	LPZ	<i>PP</i>	14	2.9	0.39	3.8	7.4
	SPZ	<i>PP</i>	1.4	0.57	0.15	3.5	3.8
	SPZ	<i>PP</i>	2.0	0.59	0.15	3.5	3.9
	LPZ	<i>LR</i>	20	1.4	0.4	3.8	3.5
South Sandwich earthquake	LPZ	<i>P</i>	8	4.3	0.44	3.4	9.8
Dominican Republic earthquake	SPZ	<i>P</i>	OBS 0.10 BDA 0.17}	0.17	0.37	3.5	0.46
	SPZ	<i>S</i>	0.8	0.41	0.37	3.5	1.1

* Ratio of the ground-motion amplitudes of the listed seismic arrival at the two sites.

† Ratio of the average microseism amplitudes measured just before the pertinent earthquake occurred.

much as 10:1 at short periods. However, the ground-motion amplitudes are larger at Bermuda for periods longer than about 3 sec. The ratio of ground motion at the BDA recording site to that for the OBS site reaches its maximum observed value (4.3) for a *P* wave of 8-sec period. For 20-sec surface waves, amplitudes measured for BDA are larger than those for OBS by a factor of about 1.4. If the surface-wave energy flux is the same at both sites, the theoretical ratio is 1.45 for the models considered here. At longer periods the signal ratio approaches 1 as the differences in structure become negligible in comparison with a wavelength.

To arrive at some measure of the relative detectability of earthquake signals at the two sites, we measured the microseismic levels present at each site just before the arrival of an earthquake and divided them into the ground-motion amplitudes of the earthquake phases. This quantity is taken to be the signal-to-noise ratio, *S/N*, at each site. A summary of these measurements is given in Table 5. As expected, OBS shows better *S/N* at high frequencies and BDA is better at low frequencies. The crossover is at approximately 1 cps. Note that the values listed in Table 5 were measured on the vertical-component seismographs. Ocean-bot-

tom *S/N* values for the horizontal components are smaller by a factor of approximately 3.5.

Seismograms for the two well-recorded distant earthquakes are shown in Figures 23 and 24. The larger amplitudes seen on the BDA records early in the surface wavetrain are explained by the greater long-period magnification of these instruments.

An interesting aspect of the ocean-bottom recording from the South Sandwich Islands earthquake (Figure 24) is the well-developed train of short-period waves which appears on the horizontal component between the *P* and *PP* phases. The predominant period of this train is 4 sec. On the BDA E-W record there is possibly some of the same phase, but it appears to be absent from both OBS and BDA Z records. This phase was not observed on any of the seismograms for the Kurile Islands earthquake. *Sykes and Oliver* [1964a, b] discuss a mode of propagation in an oceanic waveguide that may be related to this phase. They show that when a low-rigidity sediment layer is present, a type of leaking mode which results from constructive interference between *SV* waves multiply reflected in the sediment layer can exist. The phase velocities corresponding to the largest amplitudes for this mode would be expected to fall between the

compressional and shear wave velocities of the crustal layer immediately beneath the sediment layer. However, the phase velocity of the upcoming P wave, which in the present case apparently excited the observed resonance, is much higher. Hence the efficiency of generation of this phase would be expected to be low unless other effects, e.g., nonparallel layering, are involved. The predominant periods associated with waves of this mode are given approximately by

$$T_n = \frac{1}{(2n-1)} \frac{4H_2}{\beta_2} \quad n = 1, 2, 3 \dots \quad (9)$$

where T is the period, n is the mode number, and H_2 and β_2 are the thickness and shear velocity of the sediment layer. The sediments in the vicinity of the OBS site are approximately 0.3 km thick and the average shear velocity of the sediments is about 0.3 km/sec. Substituting these values into (9), we find that the corresponding period of the fundamental mode 'leaky SV ' is 4 sec, as was observed. Also, an SV wave reflecting between the boundaries of the sediment layer at nearly normal incidence will excite very little vertical motion at the water-sediment interface, which would explain the absence of this phase on the vertical-component seismographs.

A peak-for-peak correlation between the BDA and OBS seismograms is possible for the Rayleigh and Love wavetrains from the Kurile Islands earthquake. The orientation of the OBS horizontal-component seismograph was de-

termined from the amplitude and phase relations between the two sets of seismograms. The 'up' direction on the seismogram for the horizontal component was found to correspond to particle motion along an azimuth of $38^\circ \pm 10^\circ$. The theoretical difference in the ratio of horizontal-to-vertical particle motion at the two sites was accounted for in the computation.

8. SUMMARY AND CONCLUSIONS

The major findings resulting from this study are summarized in the following paragraphs.

1. Microseisms recorded on the ocean bottom in the period range of 3.0 to 5.0 sec are genetically related to those measured on a nearby island. At any given time, the predominant period of microseisms on the island is very nearly the same as that on the ocean floor, but the amplitudes are much larger on the ocean floor. The energy flux, however, is about the same at both sites.

2. The observed microseisms propagate primarily as fundamental mode Rayleigh waves. At the OBS site, the predominant direction of propagation of microseisms is from within a 180° sector which includes Bermuda. The large difference between microseismic amplitudes measured on the ocean bottom and on the surface of the Bermuda pedestal results primarily from the contrasting distribution of energy with depth for these two structures. Calculations demonstrate that for the oceanic structure, Rayleigh mode particle motion is largely confined to the water-sediment interface

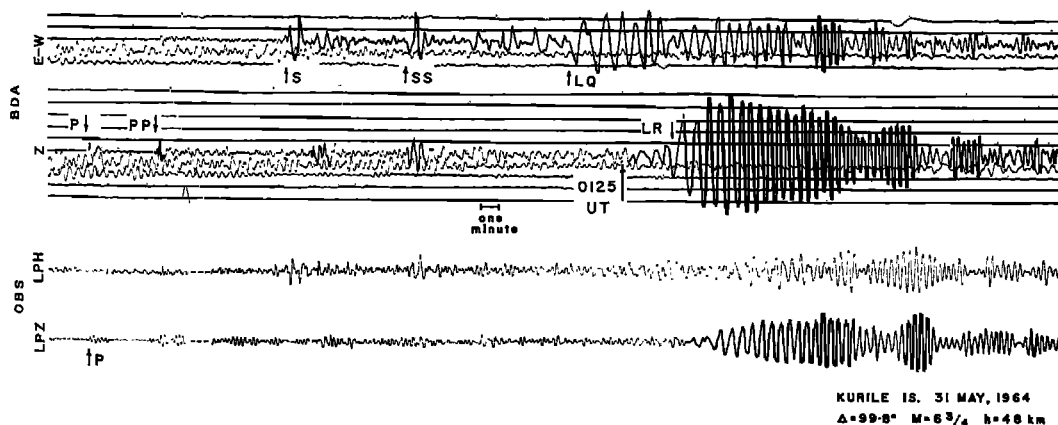


Fig. 23. Comparison between seismograms from the Bermuda standard station and the ocean-bottom instruments for an epicenter near the Kurile Islands (see Table 4).

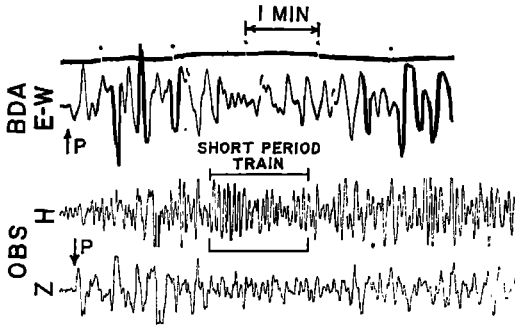


Fig. 24. Enlarged seismograms from the South Sandwich Islands earthquake showing a well-developed train of 4-sec wave on OBS horizontal component. The BDA seismogram has been enlarged 4 times relative to the OBS seismograms producing equal time scales and nearly equal magnifications at 4 sec period.

at these short periods; whereas for the Bermuda pedestal, energy is more uniformly distributed with depth, so that amplitudes at the island surface cannot be as large as those on the ocean bottom if there is the same energy flux at both sites.

3. The data indicate that microseisms with periods near 4 sec are generated by water-wave interaction near Bermuda and not directly beneath the storm systems that are the progenitors of these microseisms.

4. The characteristics of microseisms are determined by the water-wave (source) spectrum and the response function of the layered medium in which generation and propagation occur. Normally the bandwidth of the function which represents the water-wave spectrum is very narrow relative to the bandwidth of a function which properly describes the response of the layered medium; thus the water-wave spectrum will usually be the dominant factor in shaping the microseism spectrum. Q values for the spectral peaks of water waves incident on the island are approximately the same as those for concurrent microseisms.

5. There is no simple relation between the water-wave energy flux incident on the island and microseismic energy in the vicinity. Two maximums were observed for both microseisms and water waves. Although the maximums were contemporaneous, the larger microseism maximum was associated with the smaller water-wave maximum. The primary wave-generating

storm system is obvious in both cases. Weather maps were searched for other weather systems which, in conjunction with the primary disturbances, might have produced opposing swell in the vicinity of Bermuda. No secondary wave sources of this nature are evident; therefore the most likely mechanism for energy transfer in this case is the interaction between incoming water waves and those reflected from the island. The energy flux for incoming water waves is larger than the energy flux for local microseisms by a factor of approximately 10^5 .

6. An FM receiver floating on the surface, in conjunction with a single-frequency acoustic generator located on the ocean floor, makes a reliable one-dimensional wave recorder, as has been demonstrated for the relatively quiet seas encountered during this experiment (sea states 2 to 5).

7. The ground motion associated with earthquake arrivals is larger on the ocean bottom for periods shorter than 2 to 3 sec but larger on the island for longer periods. Signal-to-noise ratios are better on the ocean floor for periods shorter than about 1 sec but better at the island site for longer periods. Signal-to-noise ratios on the ocean bottom are 3 to 4 times better for the vertical component than for the horizontal component if unconsolidated sediments are present. If the thin layer of unconsolidated sediment were removed from the OBS site, the associated changes in the theoretical distribution of particle motion with depth would result, for the same flux, in a reduction of the amplitudes of microseisms at the ocean bottom by a factor of 8 for the vertical component and a factor of 94 for the horizontal component. A reduction in the background level of this magnitude would make the ocean bottom a superior recording site, relative to Bermuda, at all periods. Thus, for the purposes of optimizing detection capability, it would be worth while to search for a recording site that is relatively free of unconsolidated sediments.

8. The spectrums of the high-frequency P and S arrivals from the Dominican Republic earthquakes peak between 10 and 11 cps. The apparent velocities are 8.05 km/sec for the onset of the P_{hr} phase and 4.71 km/sec for the onset of the S_{hr} phase. These values are consistent with upper mantle velocities for the

western North Atlantic. In view of their velocities and the linearity of their travel-time curves, these phases are properly called P_n and S_n . They are characterized by a sinusoidal appearance, a duration of several minutes, and a predominant frequency which seems independent of the magnitude of the shock or its epicentral depth for the four earthquakes considered in this paper. These characteristics suggest that the high-frequency phases are guided waves, but the nature of the guide and its location are uncertain.

9. A sinusoidal train of waves with periods of 4 sec was found in the S - P interval from a large earthquake located near the South Sandwich Islands. The period of this wavetrain and its predominantly horizontal motion can be explained by constructive interference between multiply reflected SV waves in the unconsolidated sediment layer.

The mechanisms for generation and propagation of microseisms that appear to best satisfy our observations do not explain all microseisms in all period ranges. For example, *Oliver and Page* [1963], *Oliver* [1963], *Haubrich et al.* [1963], and others observed microseisms of the same period as local water waves in addition to the $1/2:1$ period relationship observed here. This suggests a mechanism of generation involving direct wave action in shallow water. *Donn* [1951] attributed short-period microseisms recorded on the east coast of the United States to cold fronts passing over the shallow water of the continental shelf. In this case, the water may be so shallow that its depth can be neglected. Atmospheric pressure disturbances can then be considered to be coupled directly into the underlying solid layers.

In earlier studies of microseisms at Bermuda, *Shurbet and Ewing* [1956] and *Carder* [1955] observed microseisms in the period range of 7 to 10 sec in addition to the 4-sec microseisms observed in this study. The former authors attribute the 7- to 10-sec microseisms to storms over the continental margin of the east coast of North America. *Carder* attributes the 4-sec microseisms to local weather conditions, as we have done here. Although an intense low-pressure system was present off Newfoundland during this study, no 7- to 10-sec microseisms were observed. Small microseisms in this period range could be masked on the OBS records by Dop-

pler-shift signal, but none was observed on records from the Bermuda standard station.

It was thought at first that amplitudes of microseisms might be very small at the ocean bottom and that it would therefore be a desirable recording site. We now know that this is not generally so, except at very short periods or possibly where there is no unconsolidated sediment. However, a picture of the particular utility of ocean-bottom recording is beginning to emerge. The following important areas of investigation may be facilitated by ocean-bottom recording:

1. Study of local submarine shocks where first arrivals are rich in high frequencies, or of more distant earthquakes if they produce high-frequency arrivals such as those from West Indies epicenters. In these cases, the signal level on the ocean bottom is an order of magnitude larger than on land and signal-to-noise ratios are also improved but not by so large a factor.

2. Study of ocean-continent or ocean-island transition zones by comparison of the spectrums of seismic phases and measurement of phase velocity between a coastal land station and an offshore ocean-bottom seismograph.

3. Study of microseisms.

4. Study of the seismicity and structure of the oceanic regions. Many small submarine earthquakes which would be recorded by a suitable ocean-bottom seismograph undoubtedly go undetected with the present array of land recorders. Ocean-bottom seismographs placed in the vicinity of known suboceanic seismic zones would better delineate these zones by micro-earthquake studies. Travel-time curves derived from suboceanic earthquakes recorded on the ocean bottom would provide a great deal of information on the structure of the oceanic crust to supplement what has been learned from refraction work at sea and from studies of surface waves that are recorded at conventional stations.

Acknowledgments. Special credit is due Professor W. Maurice Ewing, whose pioneering work and continuing enthusiastic support and direction made the present program possible.

James Dorman kindly gave us permission to use his surface-wave program, PV 7, and a second program for computation of the particle-motion profiles of Rayleigh waves. Maurice Davidson permitted us to use his programs for computa-

tion of the power-spectrum density functions. We are also indebted to Jack Oliver, Paul Pomeroy, and Lee Alsop for helpful discussions and for critically reviewing the manuscript. The contributions of William McDonald, Stamatios Thanos, David Prentiss, Charles Hubbard, Ludo Van Hemelrijck, and Charles Fuchs in designing and testing the instruments and collecting the data used in this study are gratefully acknowledged. We are indebted to Leonardo Seeber and Philip Crooke for their assistance in analyzing the data. Computing facilities were provided by the NASA Goddard Space Flight Center, Institute for Space Studies, New York. We wish to thank the United States Weather Bureau at San Juan, Puerto Rico, for weather data.

This research was supported by the Advanced Research Projects Agency under the Vela-Uniform program through the Office of Naval Research (contract Nonr-266(92)).

REFERENCES

- Biot, M., The interaction of Rayleigh and Stoneley waves in the ocean bottom, *Bull. Seismol. Soc. Am.*, **42**, 81-94, 1952.
- Biot, M., General theorems on the equivalence of group velocity and energy transport, *Phys. Rev.*, **105**, 1129-1137, 1957.
- Blackman, R., and J. Tukey, *The Measurement of Power Spectra*, 190 pp., Dover Publications, New York, 1958.
- Bradner, H., Seismic measurements on the ocean bottom, *Science*, **146**, 208-216, 1964.
- Bradner, H., and J. Dodds, Comparative seismic noise on the ocean bottom and on land, *J. Geophys. Res.*, **69**, 4339-4348, 1964.
- Bradner, H., J. Dodds, and R. Foulks, Investigation of microseism sources with ocean-bottom seismometers, *Geophysics*, **30**, 511-526, 1965.
- Carder, D., Microseisms at Bermuda, *Trans. Am. Geophys. Union*, **36**, 843-853, 1955.
- Dinger, J., Comparison of ocean-wave and microseism spectrums as recorded at Barbados, West Indies, *J. Geophys. Res.*, **68**, 3465-3471, 1963.
- Dinger, J., and D. Fisher, Microseisms and ocean wave studies at Guam, *Trans. Am. Geophys. Union*, **36**, 262-272, 1955.
- Donn, W., Frontal microseisms generated in the western North Atlantic Ocean, *J. Meteorol.*, **8**, 406-415, 1951.
- Douze, E., Rayleigh waves in short-period seismic noise, *Bull. Seismol. Soc. Am.*, **54**, 1197-1212, 1964.
- Ewing, J., and M. Ewing, A telemetering ocean-bottom seismograph, *J. Geophys. Res.*, **66**, 3863-3878, 1961.
- Ewing, J., and G. Tirey, Seismic profiler, *J. Geophys. Res.*, **66**, 2917-2927, 1961.
- Ewing, M., and J. Ewing, Sediments at proposed LOCO drilling sites, *J. Geophys. Res.*, **68**, 251-256, 1963.
- Ewing, M., and A. Vine, Deep-sea measurements without wires or cables, *Trans. Am. Geophys. Union*, **1**, 248-251, 1938.
- Hasselmann, K., A statistical analysis of the generation of microseisms, *Rev. Geophys.*, **1**, 177-210, 1963.
- Haubrich, R., W. Munk, and F. Snodgrass, Comparative spectra of microseisms and swell, *Bull. Seismol. Soc. Am.*, **53**, 27-37, 1963.
- Heezen, B., M. Tharp, and M. Ewing, The floors of the oceans, *Geol. Soc. Am. Spec. Paper* **65**, 74-76, 1959.
- Houtz, R., and J. Ewing, Detailed sedimentary velocities from seismic refraction profiles in the western North Atlantic, *J. Geophys. Res.*, **68**, 5233-5258, 1963.
- Houtz, R., and J. Ewing, Sedimentary velocities of the western North Atlantic margin, *Bull. Seismol. Soc. Am.*, **54**, 867-895, 1964.
- Isacks, B., and J. Oliver, Seismic waves with frequencies from 1 to 100 cycles per second recorded in a deep mine in northern New Jersey, *Bull. Seismol. Soc. Am.*, **54**, 1941-1979, 1964.
- Katz, S., and M. Ewing, Seismic refraction measurements in the Atlantic Ocean, **7**, *Bull. Seismol. Soc. Am.*, **67**, 475-510, 1956.
- Leet, D., D. Linchan, and P. Berger, Investigation of the T-phase, *Bull. Seismol. Soc. Am.*, **14**, 123-141, 1951.
- Linehan, D., Earthquakes in the West Indian region, *Trans. Am. Geophys. Union*, **11**, 229-232, 1940.
- Longuet-Higgins, M., A theory of the origin of microseisms, *Phil. Trans. Roy. Soc. London*, **A**, **243**, 1-35, 1950.
- Longuet-Higgins, M., Can sea waves cause microseisms? *Symp. Microseisms, Natl. Acad. Sci.-Natl. Res. Council Publ.* **306**, pp. 74-93, 1952.
- Monakhov, F., Microseisms at the bottom of the Baltic Sea in the northern part of the Atlantic Ocean, *Bull. Acad. Sci. USSR, Geophys. Ser., English Transl.*, no. **7**, 573-580, 1962.
- Nafe, J., and C. Drake, Physical properties of marine sediments, in *The Sea*, vol. **3**, edited by M. N. Hill, pp. 794-815, John Wiley & Sons, New York, 1963.
- Oliver, J., Additional evidence relating to a worldwide storm of microseisms with periods of about 27 seconds, *Bull. Seismol. Soc. Am.*, **53**, 681-685, 1963.
- Oliver, J., and J. Dorman, On the nature of oceanic seismic surface waves with predominant periods of 6-8 seconds, *Bull. Seismol. Soc. Am.*, **51**, 437-455, 1961.
- Oliver, J., and R. Page, Concurrent storms of long- and ultra-long-period microseisms, *Bull. Seismol. Soc. Am.*, **53**, 15-26, 1963.
- Phinney, R., Leaking modes in the crustal waveguide, **1**, The oceanic PL wave, *J. Geophys. Res.*, **66**, 1445-1469, 1961.
- Phinney, R., Structure of the earth's crust from spectral behavior of long-period body waves, *J. Geophys. Res.*, **69**, 2997-3017, 1964.
- Pickett, R., The Argus Island wave recorder, *In-*

- formal Manuscript Rept. 0-20-64 (unpublished manuscript), U. S. Naval Oceanographic Office, 1964.
- Prentiss, D., and J. Ewing, The seismic motion of the deep ocean floor, *Bull. Seismol. Soc. Am.*, *53*, 765-781, 1963.
- Press, F., and M. Ewing, A theory of microseisms with geologic applications, *Trans. Am. Geophys. Union*, *29*, 163-174, 1948.
- Rayleigh, Lord (John William Strutt), *The Theory of Sound*, 2nd ed., reprinted by Dover Publications, New York, vol. 1, pp. 475-480, 1945.
- Schneider, W., Ocean-bottom data collection and analysis, *Final Tech. Rept., Contract AF 19 (604)-3368*, Texas Instruments, Inc., Dallas, Oct. 1964.
- Schneider, W., and M. Backus, Ocean-bottom seismic measurements off the California coast, *J. Geophys. Res.*, *69*, 1134-1143, 1964.
- Schneider, W., P. Farrell, and R. Brannian, Collection and analysis of Pacific ocean-bottom seismic data, *Geophysics*, *29*, 745-771, 1964.
- Scholte, J., Over het verband tussen zeegolven microseismen, 1 and 2, *Verslag Akad. Amsterdam*, *52*, 669-683, 1943.
- Shurbet, D., The high-frequency *P* and *S* phases from the West Indies, *Bull. Seismol. Soc. Am.*, *52*, 957-962, 1962.
- Shurbet, D., and M. Ewing, Microseisms with periods of seven to ten seconds recorded at Bermuda, *Trans. Am. Geophys. Union*, *37*, 619-627, 1956.
- Strobach, K., Origin and properties of microseisms from the standpoint of oscillator theory, *Bull. Seismol. Soc. Am.*, *55*, 365-390, 1965.
- Sutton, G., and G. Latham, Analysis of a feedback-controlled seismometer, *J. Geophys. Res.*, *69*, 3865-3882, 1964.
- Sutton, G., W. McDonald, D. Prentiss, and S. N. Thanos, Ocean-bottom seismic observatories, *Proc. IEEE*, *53*, 1909-1921, 1965.
- Sykes, L., and J. Oliver, The propagation of short-period surface waves across oceanic areas, 1, Theoretical study, *Bull. Seismol. Soc. Am.*, *54*, 1349-1372, 1964a.
- Sykes, L., and J. Oliver, The propagation of short-period surface waves across oceanic areas, 2, Analysis of seismograms, *Bull. Seismol. Soc. Am.*, *54*, 1373-1415, 1964b.
- Thanos, S., and A. Hubbard, Two-way hydro-acoustic communications link for an ocean-bottom seismograph, *IEEE Trans. Geosci. Elec.*, in press, 1966.
- Toksöz, M., Microseisms and an attempted exploration method, *Geophysics*, *29*, 154-177, 1964.
- Tolstoy, I., Dispersion and simple harmonic point sources in wave ducts, *J. Acoust. Soc. Am.*, *27*, 897-907, 1955.
- Tolstoy, I., Resonant frequencies and high modes in layered waveguides, *J. Acoust. Soc. Am.*, *28*, 1182-1192, 1956.
- White, J., Motion product seismograms, *Geophysics*, *29*, 288-298, 1964.
- Woollard, G., Crustal structure beneath oceanic islands, *Proc. Roy. Soc. London, A*, *222*, 361-387, 1954.

(Manuscript received November 6, 1965;
revised January 28, 1966.)